TRANSNUCLEAR

CALCULATION PACKAGE

CALCULATION NO: NUH24PTH.0422	PROJECT NAME: NUHOMS® 24PTH Design
PROJECT NO: NUH 24PTH	CLIENT: Transnuclear, Inc.

CALCULATION TITLE:

Confirmatory Analysis Of Thermal Performance Of NUHOMS® HSM-H Storage Module Using A CFD Method

SUMMARY DESCRIPTION:

The NUHOMS® Horizontal Storage Module (HSM-H) is a concrete structure used to house dry shielded canisters (DSCs) containing spent nuclear fuel assemblies. This calculation provides a confirmatory evaluation of the thermal performance of the HSM-H using a computational fluid dynamics (CFD) code.

REVISION	TOTAL PAGES AND DISKS (IF ANY)	NAMES AND INITIALS OF PREPARERS & DATES	NAMES AND INITIALS OF VERIFIERS & DATES	APPROVER NAME AND SIGNATURE	APPROVAL DATE
0	43 1 CD	Gregory J. Banken 8/29/03	Larry H. Nielsen 8/29/03	Miguel A. Manrique Miguel A. Manrique	9/18/03

REVISION SUMMARY

REV.	DATE	DESCRIPTION	AFFECTED PAGES	AFFECTED DISKS
0	9/18/03	Initial Release	ALL	N/A

TABLE OF CONTENTS

LIST OF TABLES

LIST OF FIGURES

1. INTRODUCTION

1.1 Objective

The objective of this calculation is to provide a confirmatory evaluation of the thermal performance of the NUHOMS® Horizontal Storage Module (HSM-H) under bounding normal and off-normal conditions of storage. This evaluation uses a computational fluid dynamics (CFD) methodology to directly calculate the prototypical flow regime from the inlet vents to the HSM-H, through the inlet structure, around the dry shielded canister (DSC) and heat shields, and through the exit vents and back to the ambient. The analysis is conducted for steady-state conditions of 117°F ambient air and with an internal decay heat loading within the DSC of 40.8 kW.

1.2 Purpose of Revision 0

The NUHOMS® HSM-H design is based on a proven design with extensive operational experience. However, the HSM-H module incorporates several features to the basic HSM design to increase the module's thermal rating. Although the effectiveness of these design modifications was evaluated using a combination of computer (i.e., ANSYS finite element) modeling and hand calculations, it was desired to conduct a independent confirmation of the thermal performance of the HSM-H using an alternative methodology. This evaluation provides that alternative, confirmatory calculation.

1.3 Scope

This scope of this calculation is limited to the NUHOMS® HSM-H design as defined by its design drawings [6.3]. Further, the calculation is valid for a steady-state condition with an ambient condition of 117°F and an internal decay heat loading of 40.8 kW.

2. ASSUMPTIONS AND CONSERVATISMS

2.1 General Assumptions

2.1.1 The geometry of the NUHOMS® HSM-H is defined by the [6.3] design drawings.

2.1.2 Confirmation of the methodology used in the base calculations [6.1 and 6.2] for determining the thermal safety basis of the HSM-H design requires the evaluation of the thermal performance at only one operating condition. This assumption is based on the fact that the heat transfer with the HSM-H module will be proportional to the operating temperature via the Rayleigh number and the computed radiative heat exchange factors. As such, confirmation of this proportionality is only required at a single ambient condition.

2.1.3 The ambient condition chosen for the confirmatory calculation is the off-normal storage condition with a peak ambient temperature of 117°F. However, per the [6.1] analyses, a steady-state, 24-hour average ambient temperature of 105°F can be used to bound the thermal performance of the HSM-H module after the daily temperature range is considered.

2.1.4 The design decay heat loading for the HSM-H is 40.8 kW. The analysis assumed this heat loading was equally distributed over the minimum canister length between the top and bottom shield plugs of 169.6".

2.1.5 Since the analysis conservatively assumes an HSM-H that is located within array of HSM-H modules, solar loading will only affect the roof and front face of the HSM-H. Per the [6.2] analyses, the 24-hour average insolation on the roof will be 0.8537 Btu/hr-in^2, while the 24-hour average insolation on the front face will be 0.2134 Btu/hr-in^2.

2.2 Conservatisms

2.2.1 The minimum length of DSC that can be housed within the HSM-H is considered for the purposes of this calculation.

2.2.2 The heat transfer between the DSC and the DSC support rail structure in the HSM-H is conservatively ignored for the purposes of this calculation.

2.2.3 For simplicity and conservatism, the fins on the side heat shields are not simulated. This modeling approach will yield conservatively high temperatures for the heat shields and have a slight, but conservative, effect on the predicted DSC temperatures.

2.2.4 Also for simplicity, the additional 8 inches of stack height represented by the roof shield caps over the exit openings has conservatively been ignored. However, the loss factors associated with the flow turn and screened opening have been included as a flow resistance element in the modeling.

3. HSM-H DESIGN

3.1 HSM-H Geometry

Figure 3-1 illustrates the typical HSM-H storage array. It is typical to place the modules in a side-by-side and back-to-back arrangement to conserve ground space and maximize self-shielding. As a result of this arrangement, only the top and front faces of the interior modules will be exposed to the ambient. This limited exposure to the ambient is acceptable since the majority of the cooling of the DSC within the HSM-H occurs as the result of airflow drawn through the module via the 'chimney effect'. The airflow path through the HSM-H starts by the air being drawn in through the screened openings at the bottom of the front face of the module and traveling along both sides of the module (see Figure 3-2). The airflow enters the HSM-H cavity by turning and passing under the module sidewalls. Once in the cavity, the air flows upward around the DSC and the side heat shields before passing through the louvered heat shield at the top of the cavity. After exiting the louvered heat shield, the airflow turns horizontal and flows under the roof slab and over the top of the sidewalls, turns vertical to flow along the sides of the roof slab before finally exiting the module at the screened opening (see Item 5 in Figure 3-1).

Figure 3-3 presents the layout and dimensioning of the module's base unit, while Figure 3-4 illustrates the elevation view of the DSC support structure. As seen from Figure 3-4, each support rail has twelve 6-inch diameter holes to allow the cooling air to pass through the rail. This reduces the potential for a 'dead air' region at the bottom of the DSC.

3.2 Material Properties

The material properties used for this analysis are taken from the [6.1] and [6.2] calculations. Specifically, a thermal conductivity of 1.15 Btu/hr-ft-°F, a density of 145 lbm/ft^3, a specific heat of 0.22 Btu/lbm-°F, and an emissivity of 0.9 is assumed for the concrete. The Type 304 stainless steel used for the DSC shell, portions of the heat shields, and the DSC support structure assumes a thermal conductivity of 10.4 Btu/hr-ft-°F, a density of 501 lbm/ft^3, a specific heat of 0.121 Btu/lbm-°F, and an emissivity of 0.46. The Type 1100 aluminum used for the heat shields assumes a thermal conductivity of 128.5 Btu/hr-ft-°F, a density of 169 lbm/ft^3, and a specific heat of 0.22 Btu/lbm-°F. The anodized side of the aluminum sheet has an assumed emissivity of 0.80, while the non-anodized side of the aluminum panel has an assumed emissivity of 0.10. The soil between the base mat of the HSM-H module and the constant earth temperature of 70°F has an assumed thermal conductivity of 0.1728 Btu/hr-ft-°F and a specific heat of 0.191 Btu/lbm-°F. For simplicity and given the relatively small change, these properties are assumed to be constant with temperature.

In contrast, temperature dependant thermal properties for air are used. The thermal properties for air, as taken from the [6.1] and [6.2] calculations, are as follows:

Temperature	Density	Specific Heat	Conductivity	Viscosity
F	lbm/in^3	Btu/lbm-°F	Btu/hr-ft-°F	lbm/in-s
80	4.20E-05	0.2405	0.0152	1.04E-06
260	3.15E-05	0.2422	0.0194	1.29E-06
440	2.52E-05	0.2460	0.0233	1.51E-06

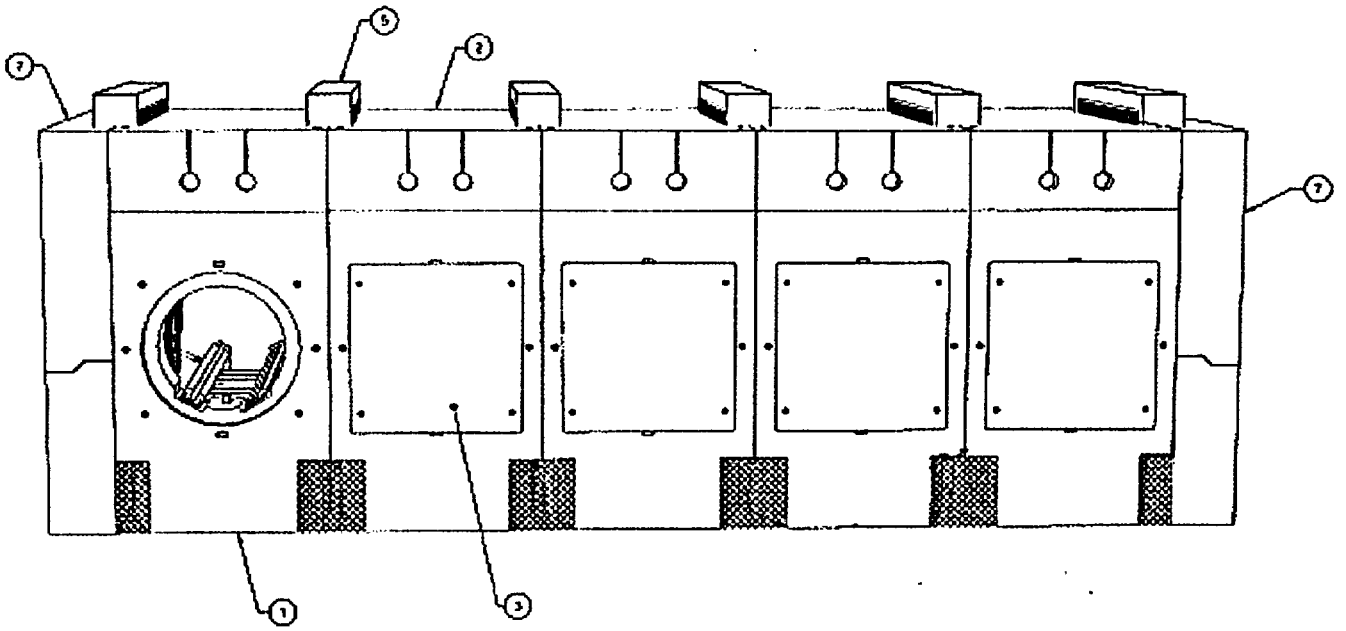

Figure 3-1 - Illustration of Typical NUHOMS HSM-H Storage Array

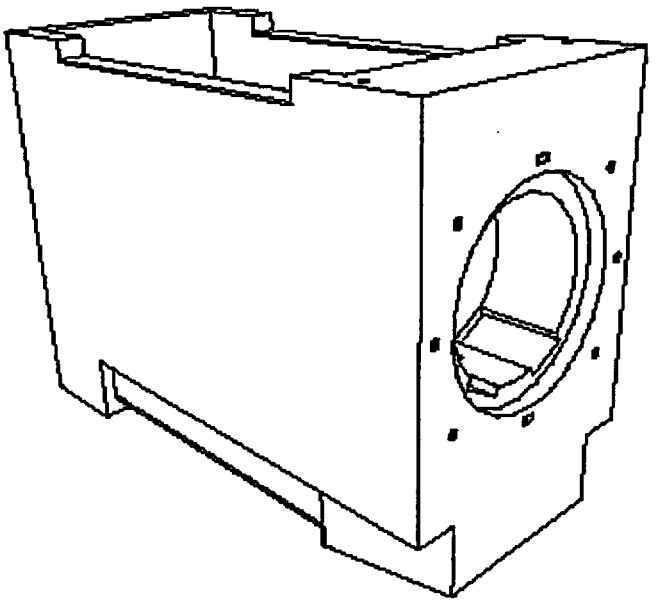

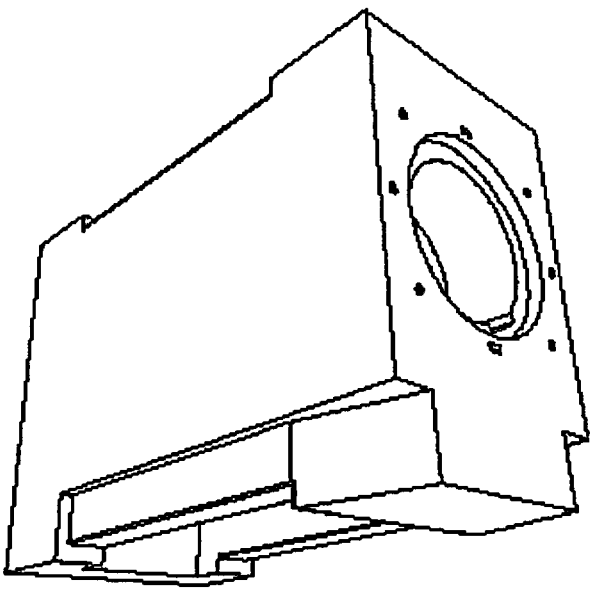

Figure 3-2 - Perspective Views Of HSM-H Base Unit

Figure Withheld Under 10 CFR 2.390

Figure 3-3 - Elevation Views Of HSM-H Base Unit

3-2-cal-00

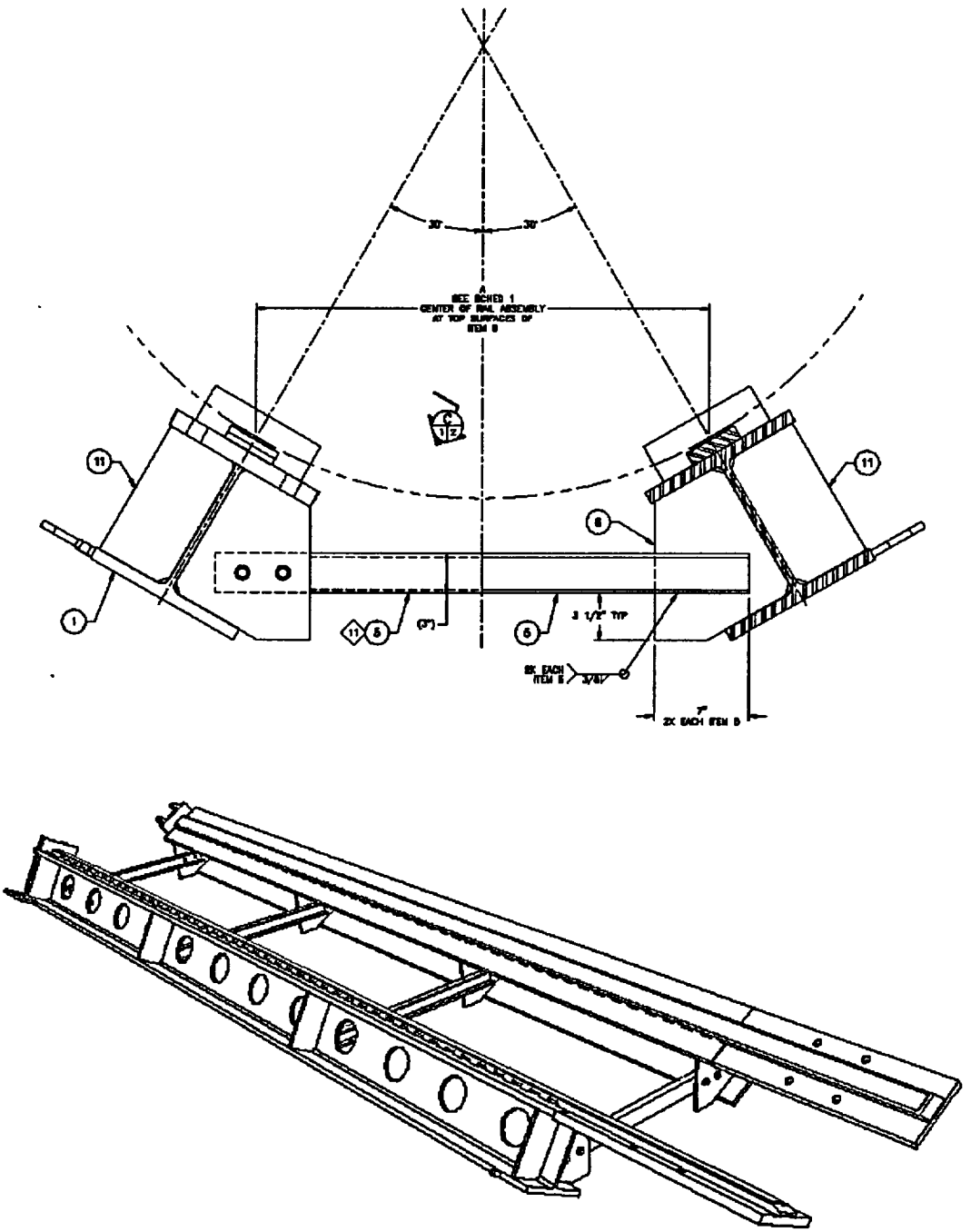

Figure 3-4 - Elevation & Perspective Views Of DSC Support Structure

4. CALCULATIONS

4.1 Fluent™/ Icepak™ Model

Based on the HSM-H geometry summarized in Section 3.1 and detailed in the [6.3] drawing set, the thermal-hydraulic environment within the HSM-H storage module was evaluated for an ambient condition of 117°F and a DSC decay heat loading of 40.8 kW. The program selected for this evaluation is the Fluent™ code [6.6] with the Icepak™ module [6.7]. The Fluent™ code is a general purpose CFD code that is recognized internationally as one of the premier codes in its class. The general modeling capabilities of the code as they relate to this application include:

- Meshing flexibility using structured and unstructured mesh generation with hexahedra, non-hexahedra, and tetrahedral mesh types
- Capability to model low speed, buoyancy driven flow regimes
- Steady-state and transient flows
- Inviscid, laminar, and turbulent flows
- Heat transfer including forced, natural, and mixed convection, conjugate heat transfer, as well as several radiation models
- Custom materials property database
- Integrated problem set-up and post-processing

The Icepak™ module is a fully interactive, object-based graphical interface that serves as pre- and post-processor to the Fluent™ code. While the Icepak™ module is specifically designed for the analysis of electronic enclosures, its operational features are fully capable of handling the geometry for this application. The verification and validation of the codes for the computation of the convection process within an enclosure is documented in [6.8].

Figure 4-2 illustrates the elevation and isometric wire frame views of the thermal-hydraulic model developed for this evaluation. The +x axis of the model's coordinate system extends across the width of the module from left to right when facing the front of the module. The +y axis is aligned with the elevation of the module with the 0 dimension at the top of the base mat and the maximum dimension at the top of the module's roof. The +z axis extends from the back of the module to the front face of the module. As seen from the solid shaded depiction in Figure 4-3, the model accurately captures the geometry of the inlet and flow structure along the sides of the model. While a symmetry plane can be assumed along a y-z plane through the center of the module, a full 3-D model is used since radiative exchange is a major heat transfer mode within the HSM-H module and the correct calculation of the view or shape factors could not be made using a symmetry model.

The concrete walls and roof of the module are modeled using a combination of polygon blocks. Figure 4-4 and Figure 4-5 illustrate the modeled geometry of the side and back walls of the module. Five separate blocks are used for each side wall model, while four blocks are used to capture the geometry of the back wall. The program automatically handles the thermal connections between the

various modeling blocks. In a similar fashion, the front wall and the roof structure are modeled using three polygon blocks each.

The modeling of the DSC within the HSM-H module (see Figure 4-6) is accomplished using 3 cylindrical blocks. These are a 7.45-inch long solid block representing the bottom closure plug, a 8.95-inch long solid block representing the top closure plug, and a 169.6-inch long hollow block representing the 0.5-inch thick shell of the DSC over the length of the fuel basket. Since the fuel basket is not specifically modeled, the decay heat loading is simulated as a uniform heat flux applied over the 169.6-inch length of the DSC shell between the closure plugs. For conservatism, the minimum DSC length is assumed for the analysis.

Figure 4-7 illustrates the model geometry for the heat shields within the HSM-H. The heat shields are modeled using thin conducting plate elements. For simplicity and conservatism, the fins on the side heat shields are not simulated. This modeling approach will yield conservatively high temperatures for the heat shields, but have only a slight and conservative effect on the predicted DSC temperatures. The louvered heat shield at the roof of the HSM-H module is modeled as a series of 79 individual plates in order to accurately capture the geometry, and thus the flow regime through the louvers. Figure 4-8 provides an enlarged view of Figure 4-7 illustrating the placement of the individual, angled plates used to simulate the louvered shield. In each case, the side of the heat shield facing the DSC is assumed to be anodized aluminum, while the side facing the concrete structure is assumed to have an non-anodized surface finish.

The rails supporting the DSC within the HSM-H are modeled as resistance type elements. This model element type provides the ability to simulate the flow restriction imposed by the presence of the support rails, without the need of modeling the individual holes in the rails. The same flow loss coefficient used in the [6.1] analysis (i.e., 113.5 based on approach velocity) is used for this evaluation. Likewise, the final flow turn before the outlet opening and the wire mesh at the screened opening is not specifically modeled in order to simplify the modeling and since the flow losses associated with these items are well defined by previous work (.i.e., [6.5], etc.). Instead, the combined flow loss factors used in the [6.1] analysis for these items (i.e., 1.41, based on approach velocity) are applied as a flow resistance element at the outlet.

The ability of the Fluent™ program to create unstructured computational meshes was used to concentrate the mesh density in those areas requiring greater fluid flow and/or thermal resolution and decrease the mesh density in those areas (i.e., within the concrete walls, etc.) that do not experience large gradients. The resultant unstructured mesh used for this evaluation is illustrated in Figure 4-9 to Figure 4-16. Figure 4-9 and Figure 4-10 present the perspective and elevation views of the mesh profile along the x-y plane through the center of the module, while Figure 4-11 presents the perspective view of the mesh profile along the y-z plane through the center of the module. The unstructured nature of the mesh is evident from the figures with the mesh density being significantly higher in the region of the DSC shell, heat shields, and the outlet vents and lower elsewhere.

Further evidence of the unstructured nature of the mesh used in the modeling can be seen by comparing the mesh layout at the front wall of the module as illustrated in Figure 4-12, with the mesh layout illustrated in Figure 4-9. As a global control over the development of the mesh, the maximum element size is limited to 3 inches in the x-direction, 6-inches in the y-direction, or 8-inches in the z-direction. The total size of the mesh used in the modeling exceeds 1,629,250 elements.

Figure 4-13 illustrates an enlarged view of the meshing in the vicinity of the louvered shield. The mesh density provides approximately 4 mesh elements between each set of plates making up the shield and 6 mesh elements through the height of the louver. The same mesh density is provided in a region extending ½ inch below and 6 inches above the louvers. The enlarged view illustrated in Figure 4-14 shows the mesh in the vicinity of the DSC, through the thickness of the DSC shell, and around the DSC support rails. Figure 4-15 illustrates the meshing in at the exit vents, while Figure 4-16 illustrates the mesh layout in the vicinity of the inlet vents.

Direct simulation of insolation on the outer surface of the HSM-H could not be included in the selected modeling approach due to program limitations on the number of boundary conditions that could be applied. Therefore, the simulation of the insolation was addressed by increasing the ambient condition used to compute the convective and radiation heat transfer exchange from the affected surfaces. Based on past experience, this temperature increase was estimated to be 35°F for heat exchange with the exterior surface of the roof (i.e., from 105°F to 140°F) and 25°F for heat exchange with the front face of the module (i.e., from 105°F to 130°F). Adiabatic conditions are assumed for the side and back walls of the module.

4.2 Confirmatory Analysis

Figure 4-17 to Figure 4-22 present a summary of the surface temperature distributions predicted for the analyzed decay heat loading of 40.8 kW within the DSC and the assumed bounding 24-hour average ambient condition of 105°F. The equivalent results from the [6.2] analysis is presented Appendix B.

Figure 4-17 illustrates the predicted temperature profile on the DSC surface. As seen, the maximum surface temperature predicted is 428°F. Comparison with the equivalent results from the [6.2] analysis is presented Appendix B shows that the CFD predicted temperature variation around the circumference of the DSC does not uniformly increase from the bottom to the top of the shell as predicted by the [6.2] analysis. The reason for this result is two fold. First, the conduction between the DSC and the support rail is conservatively ignored for the CFD analysis, but the negative impact from the flow blockage imposed by the rails is not. As such, the predicted temperatures for the lower portion of the DSC shell are hotter than the expected actual levels, which in turn skews the circumferential profile. Second, the CFD analysis shows that the velocity profile around the DSC is not constant. As such, the convection coefficient will vary accordingly, yielding varying local surface temperatures. Since the decay heat load is being applied as a surface heat flux, small variations in local conditions will result in relatively large changes in local temperatures. In reality, the heat

transfer within the DSC shell and fuel basket due to the aluminum plates and rails will smooth out these surface temperature variations and, when combined with credit for heat transfer into the support rails, could be expected to yield a more uniform increase in temperature from the bottom of the DSC to the top.

Figure 4-18 illustrates the temperature profile on the heat shields within the HSM-H module. Comparison with the [6.2] analysis results presented Appendix B shows that both the temperature levels achieved and the location of the maximum temperature points are different. The higher temperatures predicted for the side heat shields by the CFD analysis are directly related to the ignoring of the fins on the shields. Inclusion of these fins in the CFD analysis would significantly increase the area available for convective heat transfer and reduce the peak temperature levels predicted. The difference in the location of the peak temperature points is due to the [6.2] analyses' assumption of a uniform air flow distribution within the HSM-H, whereas the CFD analysis directly calculates the distribution of air flow and its associated change in local temperature and convection coefficient. The same conclusion is true for the louvered heat shield at the top of the HSM-H module (see Figure 4-19).

The concrete wall temperature distribution depicted in Figure 4-20 for the base unit is comparable to the equivalent profile from the [6.2] analysis results presented in Appendix B. Both analyses predict a peak concrete temperature in the range of 200°F and both analyses predict approximately the same location for the occurrence of the peak temperature (i.e., near the top of the rear wall of the module). However, as seen from Figure 4-21 and Figure 4-22, the CFD analysis predicts a peak roof concrete temperature that is approximately 25°F hotter than the [6.2] analysis. The reason for this difference is thought to be partially due to differences in the computed view factors between the DSC and the underside of the roof through the louvered heat shield and partially due to differences in the flow distribution within the HSM. The [6.2] analysis assumes a fully mixed air temperature within each of its nine fluid zones, while the CFD analysis includes a 'plume' of hot air rising up from the centerline of the DSC and striking the roof's underside before mixing with the air near the edges of the module.

Figure 4-23 to Figure 4-26 present a sampling of the flow velocity profiles within the HSM-H module. Figure 4-23 illustrates the profiles along two x-y planes through the module. As seen, the maximum velocity within the HSM-H occurs that the end of the converging inlet structure since this location presents the minimum flow area. Further, an area of flow circulation can be noted below the DSC due to the combined effects of the side inlet inflow and the flow resistance from the DSC support rail structure. This region of flow circulation is also evident in Figure 4-24, which presents the velocity profile along a x-y plane through the center of the module.

An enlargement of the Figure 4-24 profile in the vicinity of the support rails is shown in Figure 4-25. The flow resistance created by the support rails is evident in depicted velocity vectors.

Figure 4-26 presents an enlargement of the Figure 4-24 profile in the vicinity of the louvered heat shield and entrance to the exit vents.

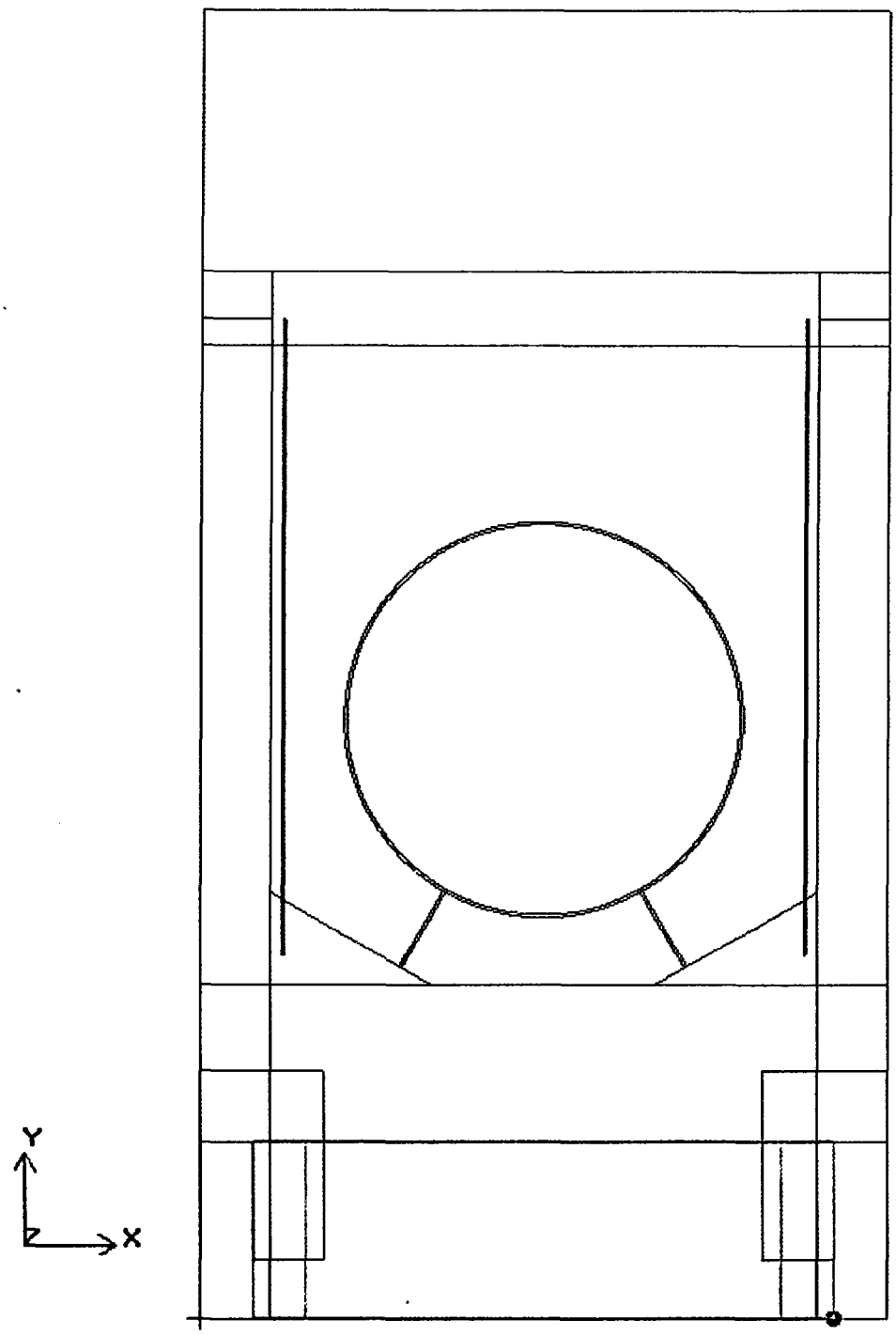

Figure 4-1 - Elevation View Of Model Layout

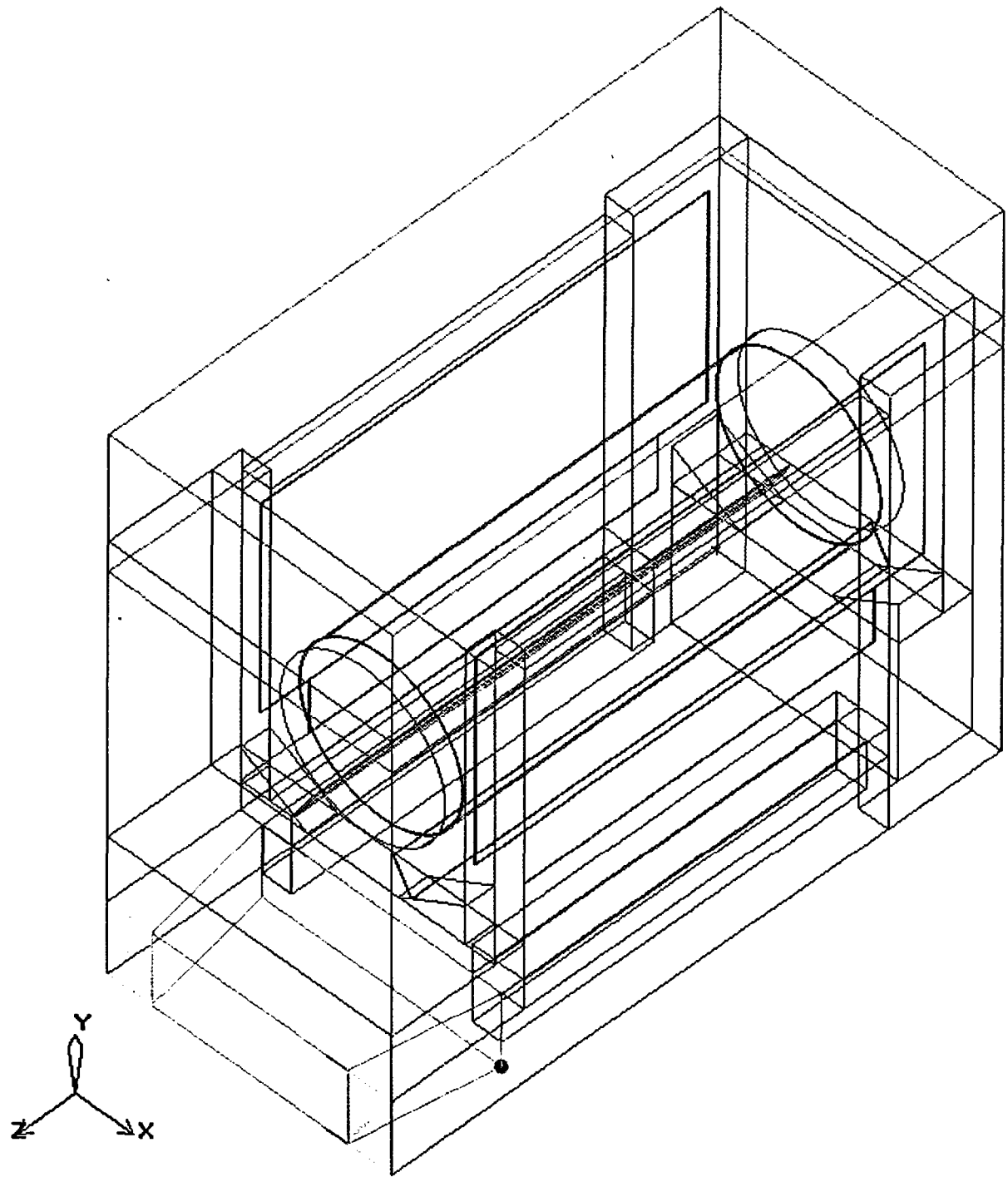

Figure 4-2 - Isometric View Of Model Layout

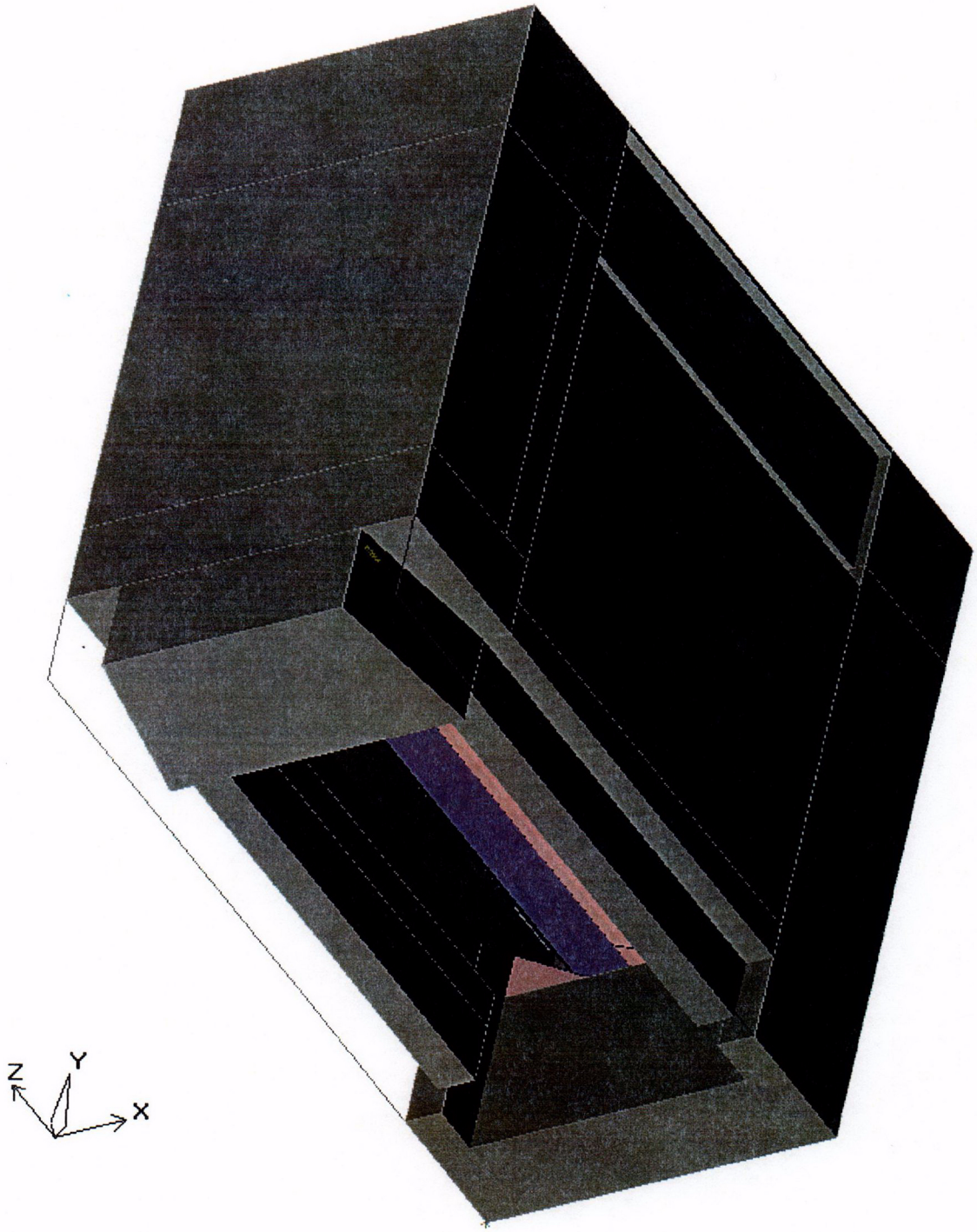

Figure 4-3 - Model View From Underside Of HSM-H

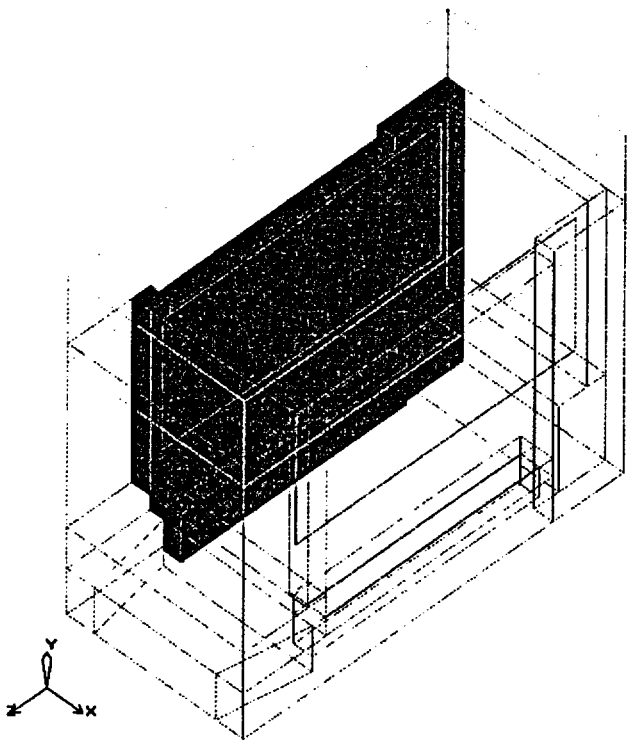

Figure 4-4 - HSM-H Sidewall

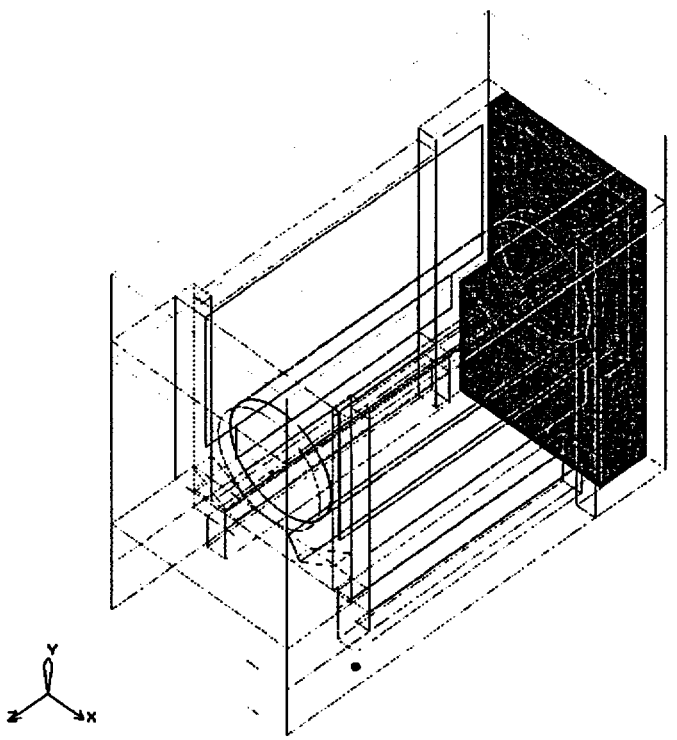

Figure 4-5 - HSM-H Backwall

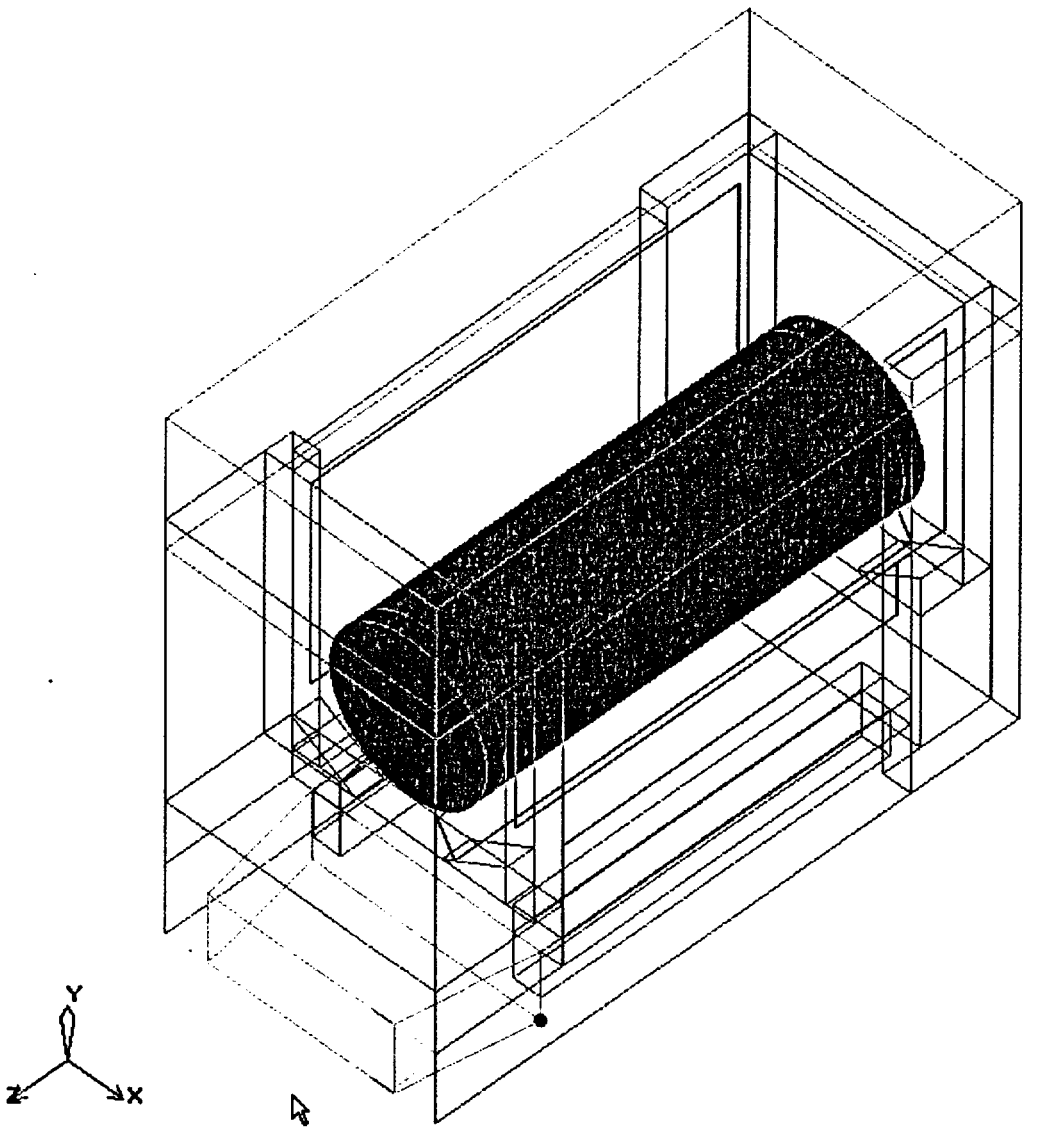

Figure 4-6 - DSC Within HSM-H

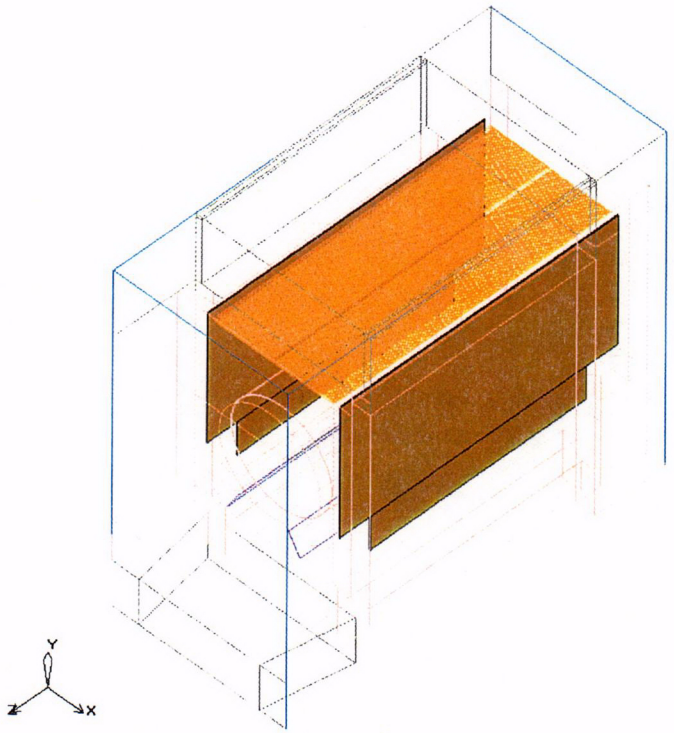

Figure 4-7 - Heat shields Within HSM-H

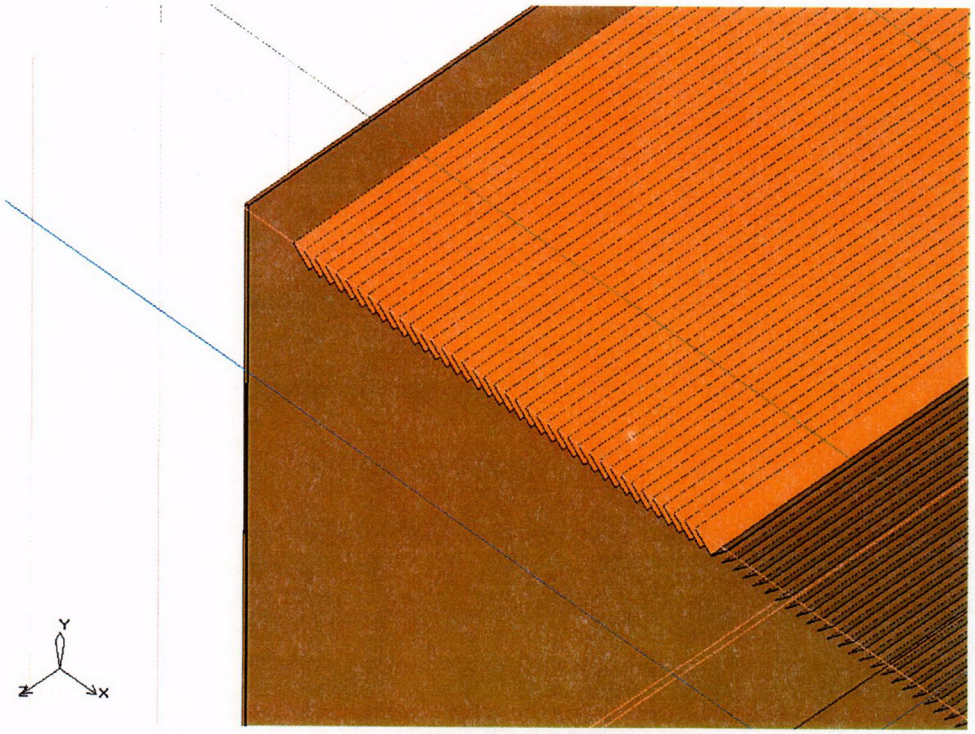

Figure 4-8 - Enlarged View Illustrating Use Of Individual Plates To Model Louvered Heat shield

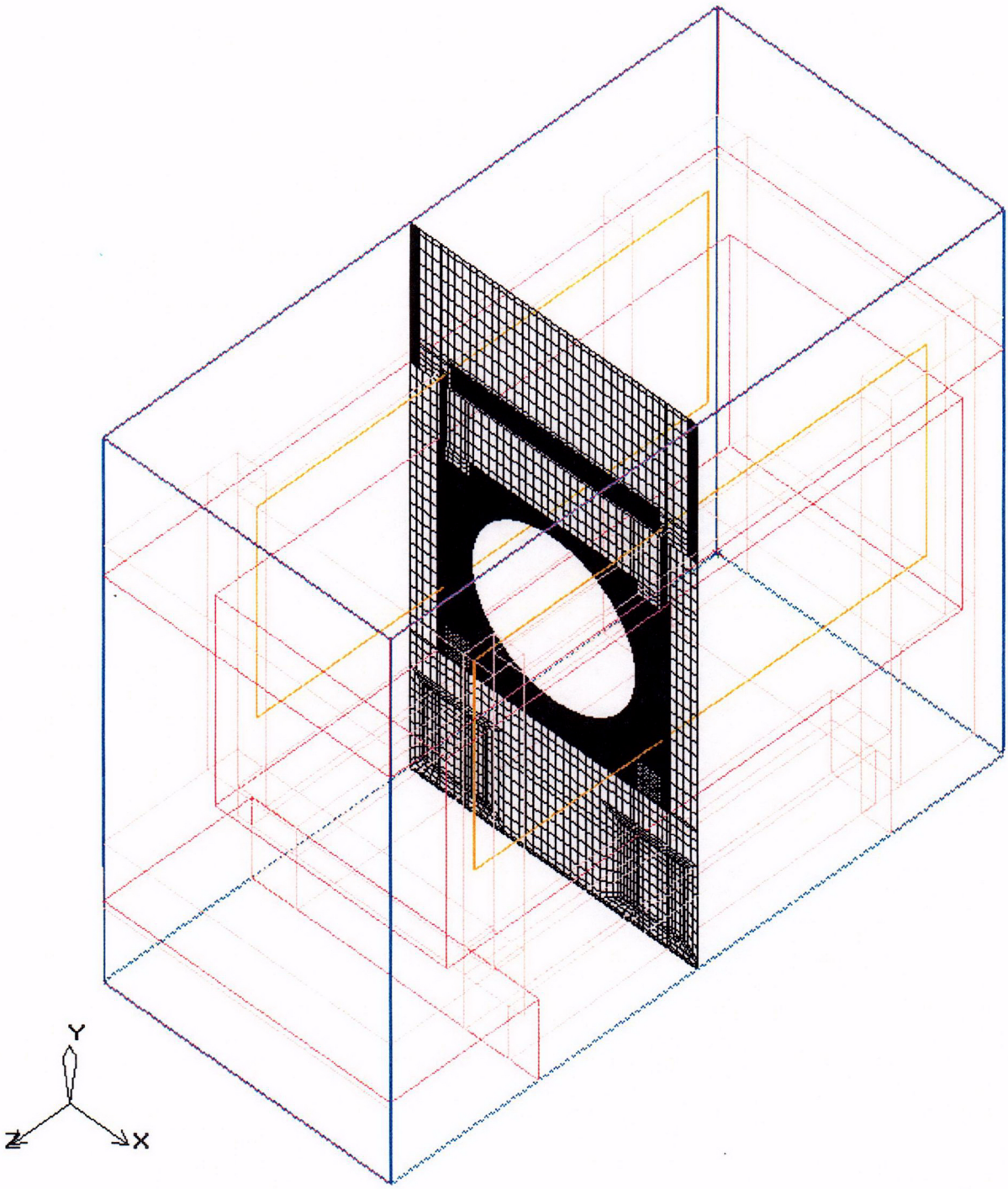

Figure 4-9 - Perspective View Of Meshing At X-Y Plane Of HSM-H

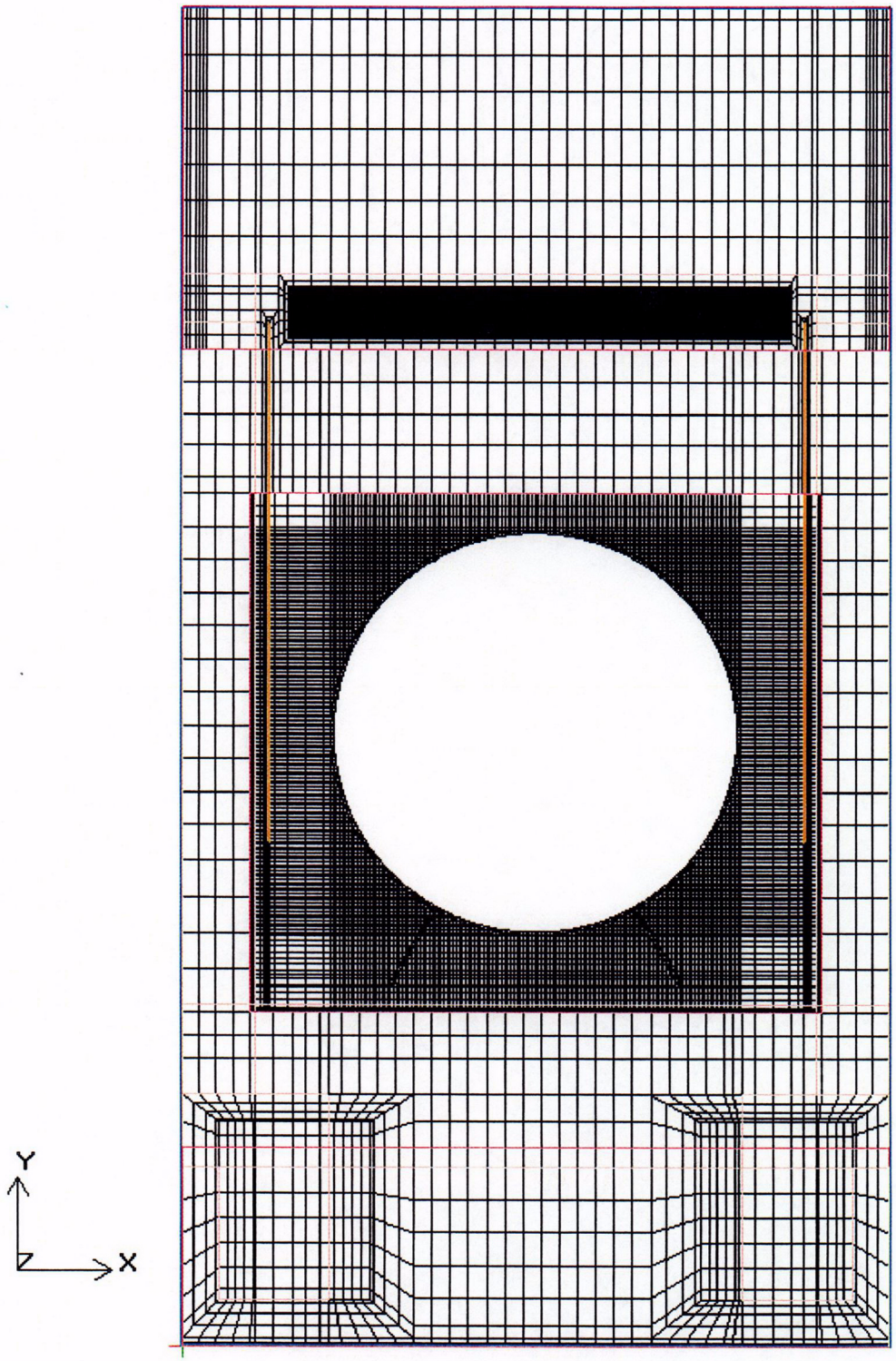

Figure 4-10 - Elevation View Of Meshing At Center Of HSM-H

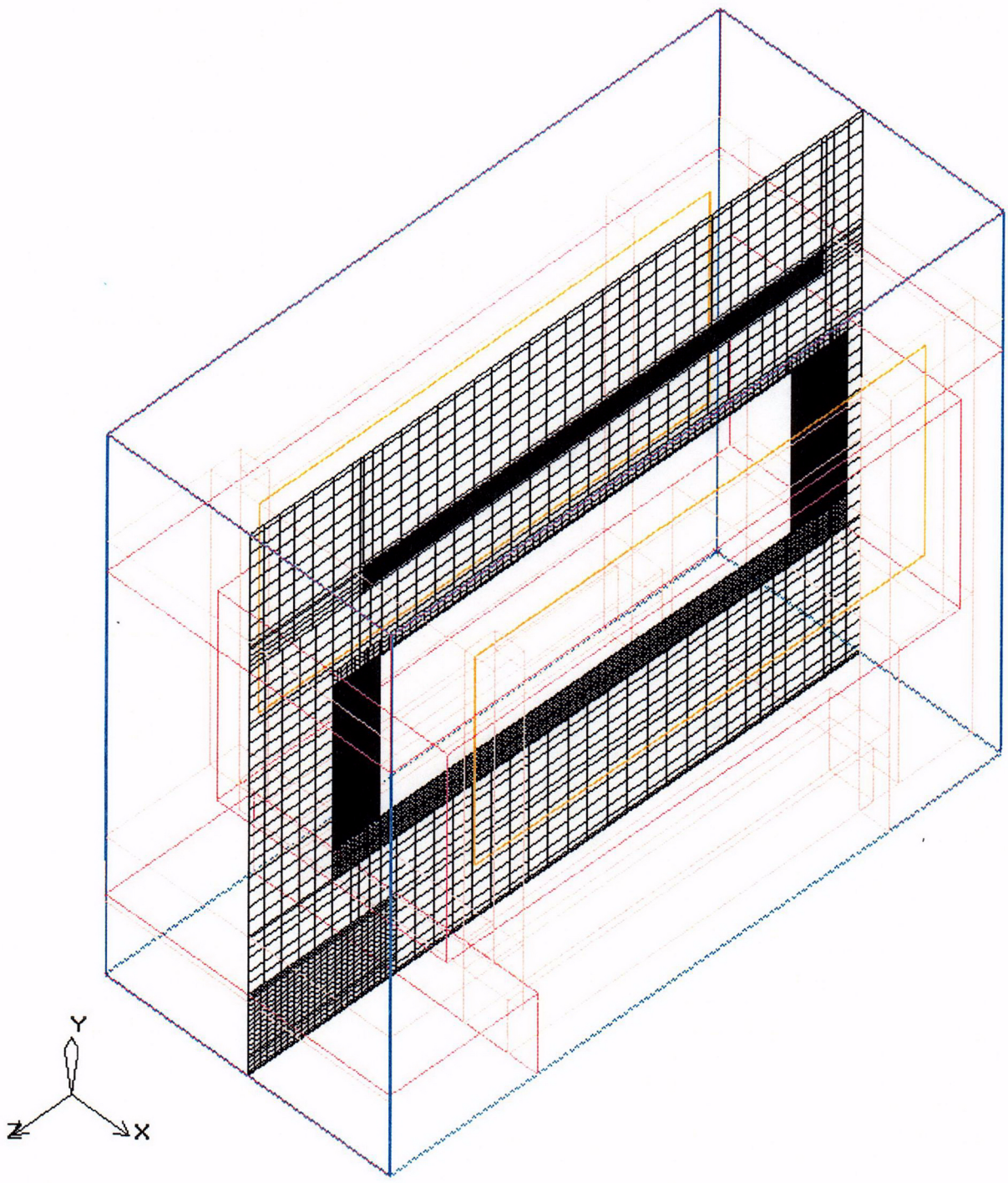

Figure 4-11 - Elevation View Of Meshing At Z-Y Plane Of HSM-H

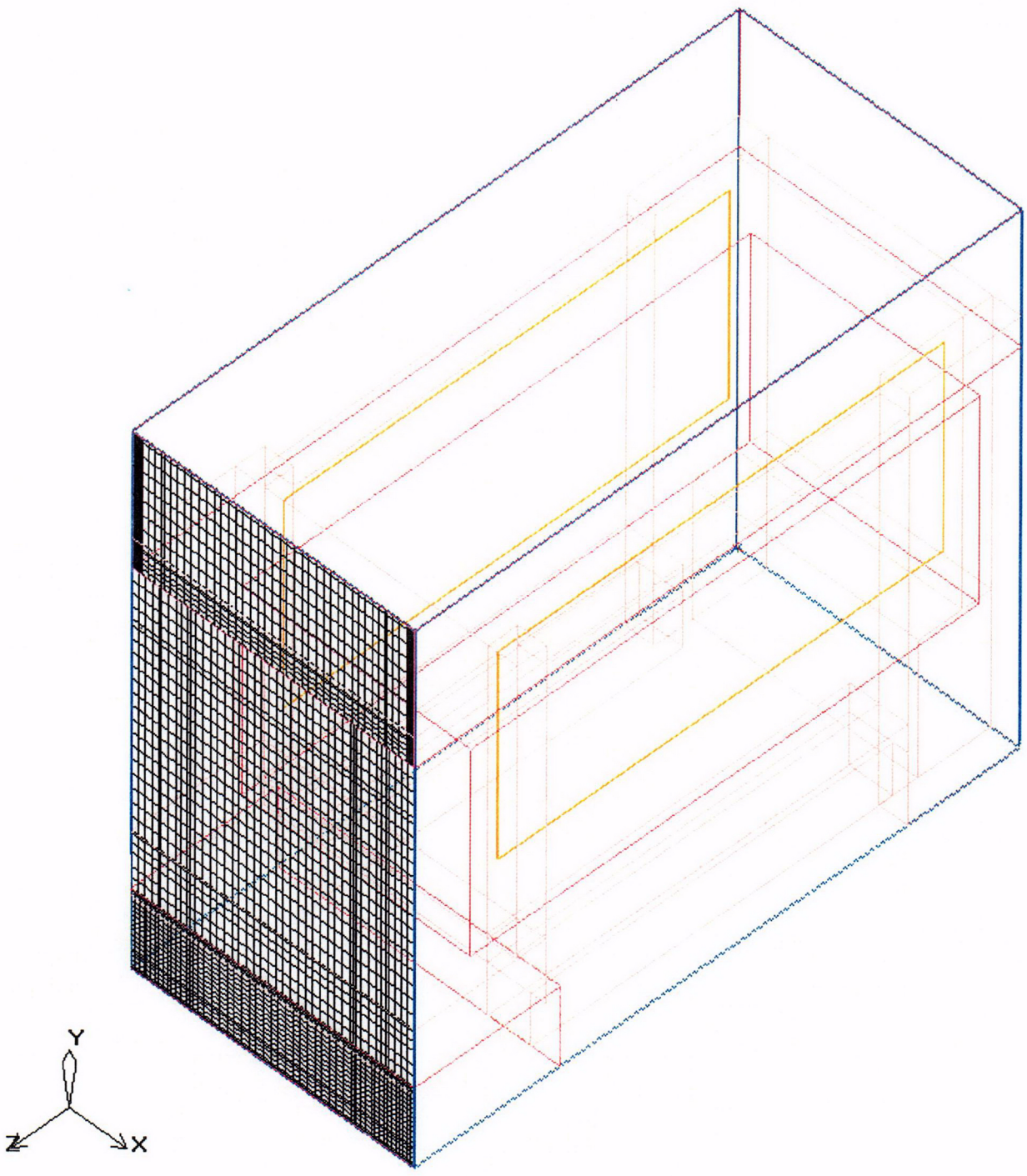

Figure 4-12 - Perspective View Of Meshing At Front Edge Of HSM-H

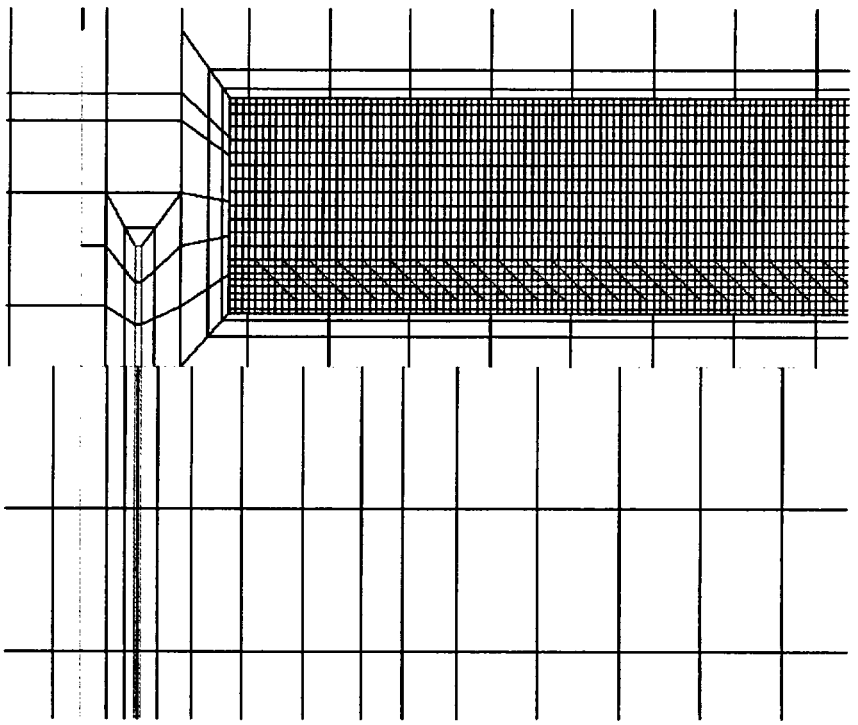

Figure 4-13 - Enlarged View Of Meshing At Roof Of HSM-H

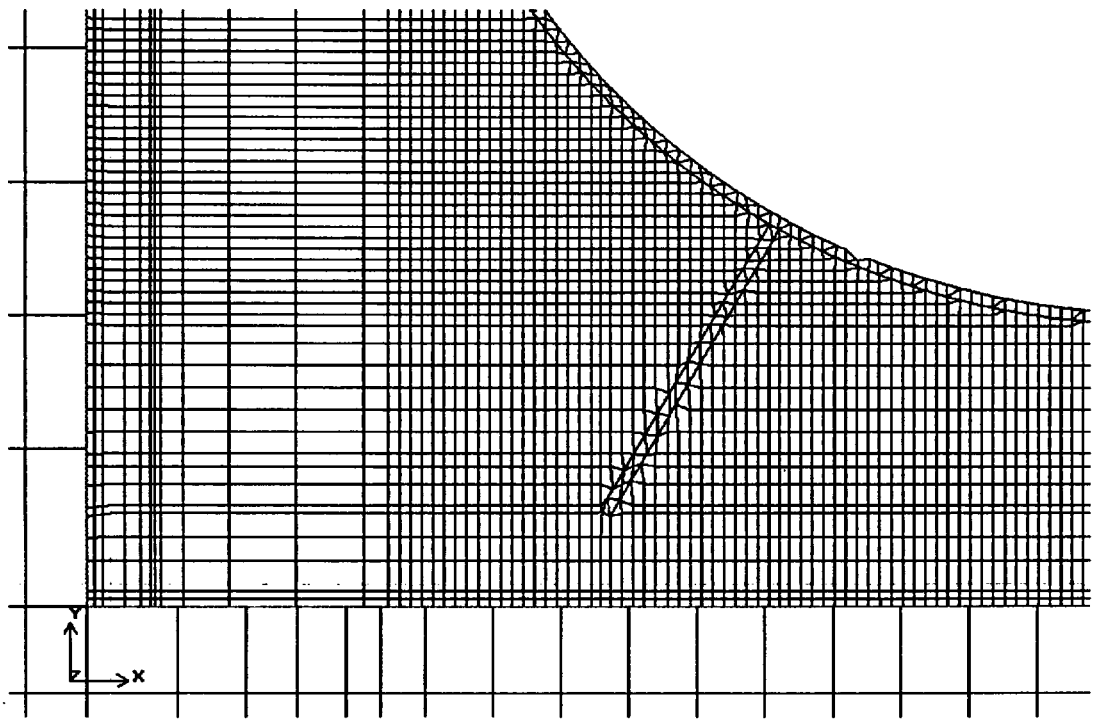

Figure 4-14 - Enlarged View Of Meshing At DSC Support Structure

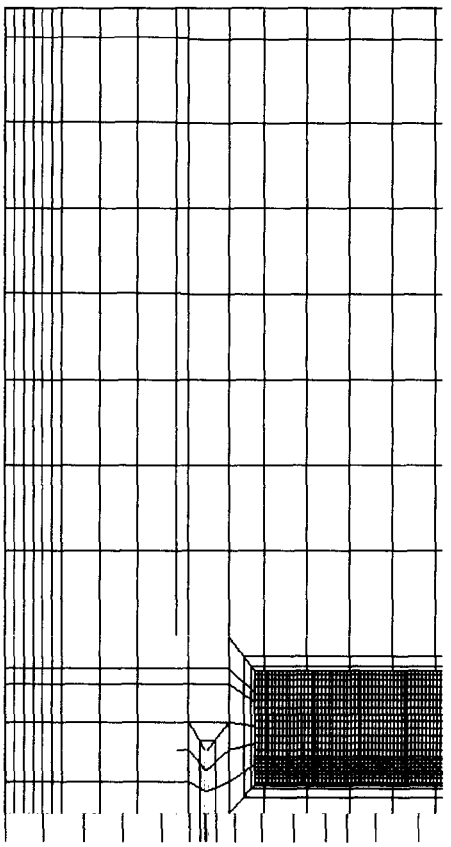

Figure 4-15 - Enlarged View Of Meshing At Outlet Vents

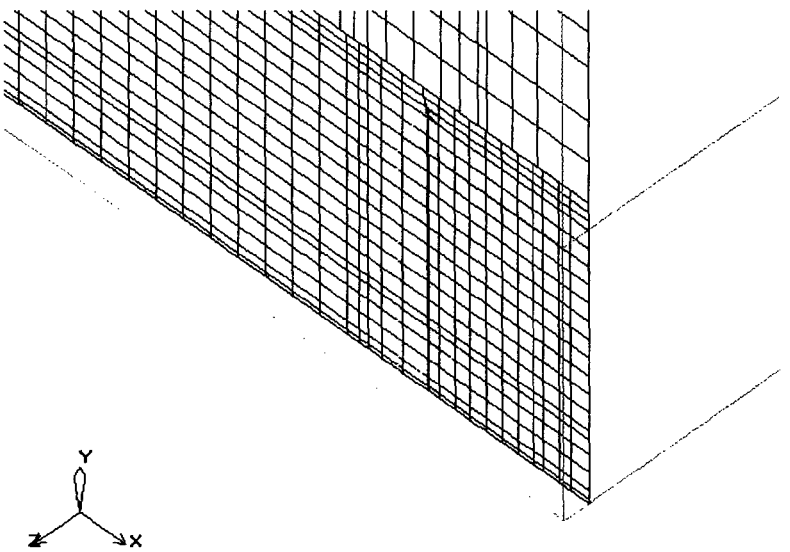

Figure 4-16 - Enlarged View Of Meshing In Vicinity Of Inlet Vents

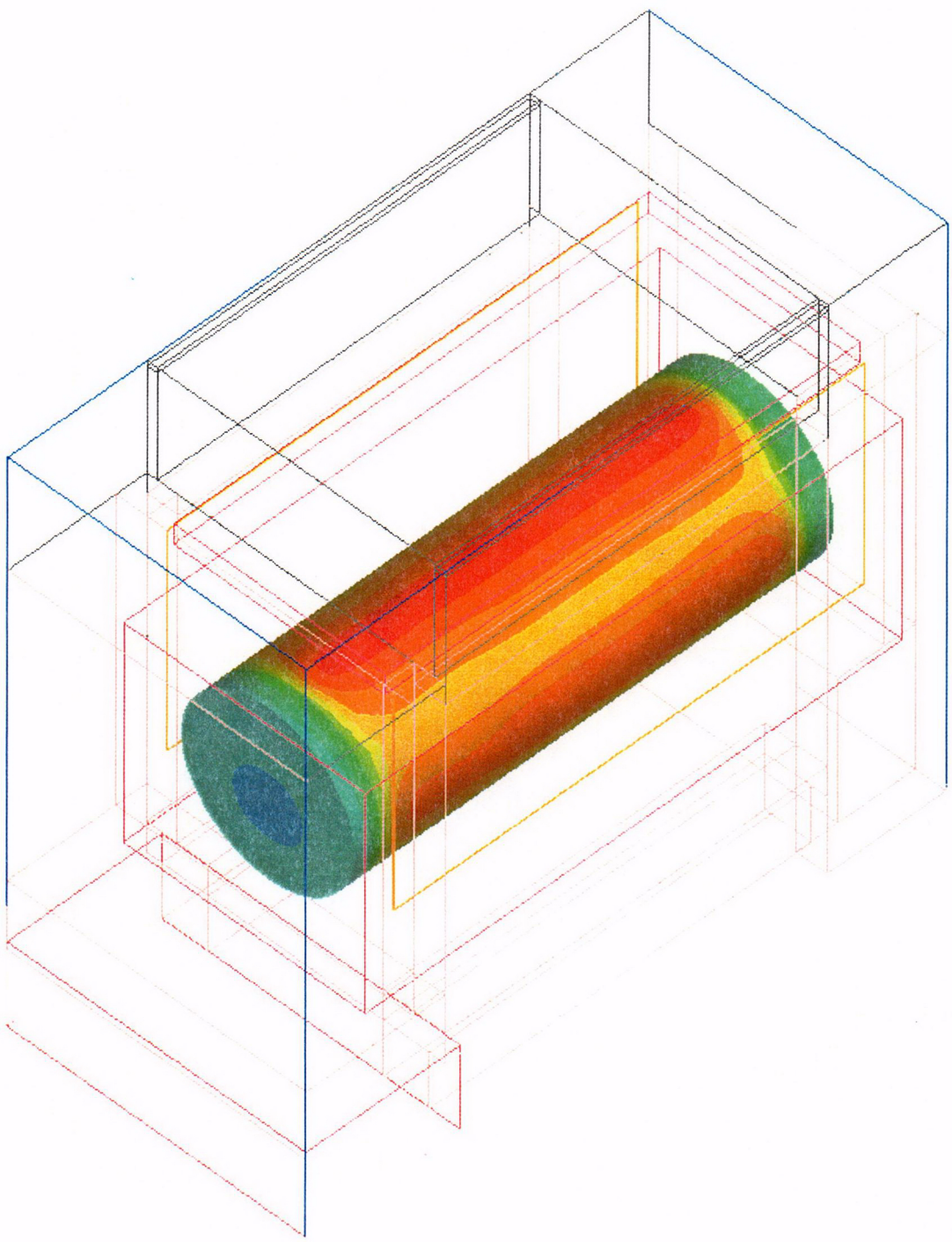

Figure 4-17 - Temperature Distribution On DSC Surface

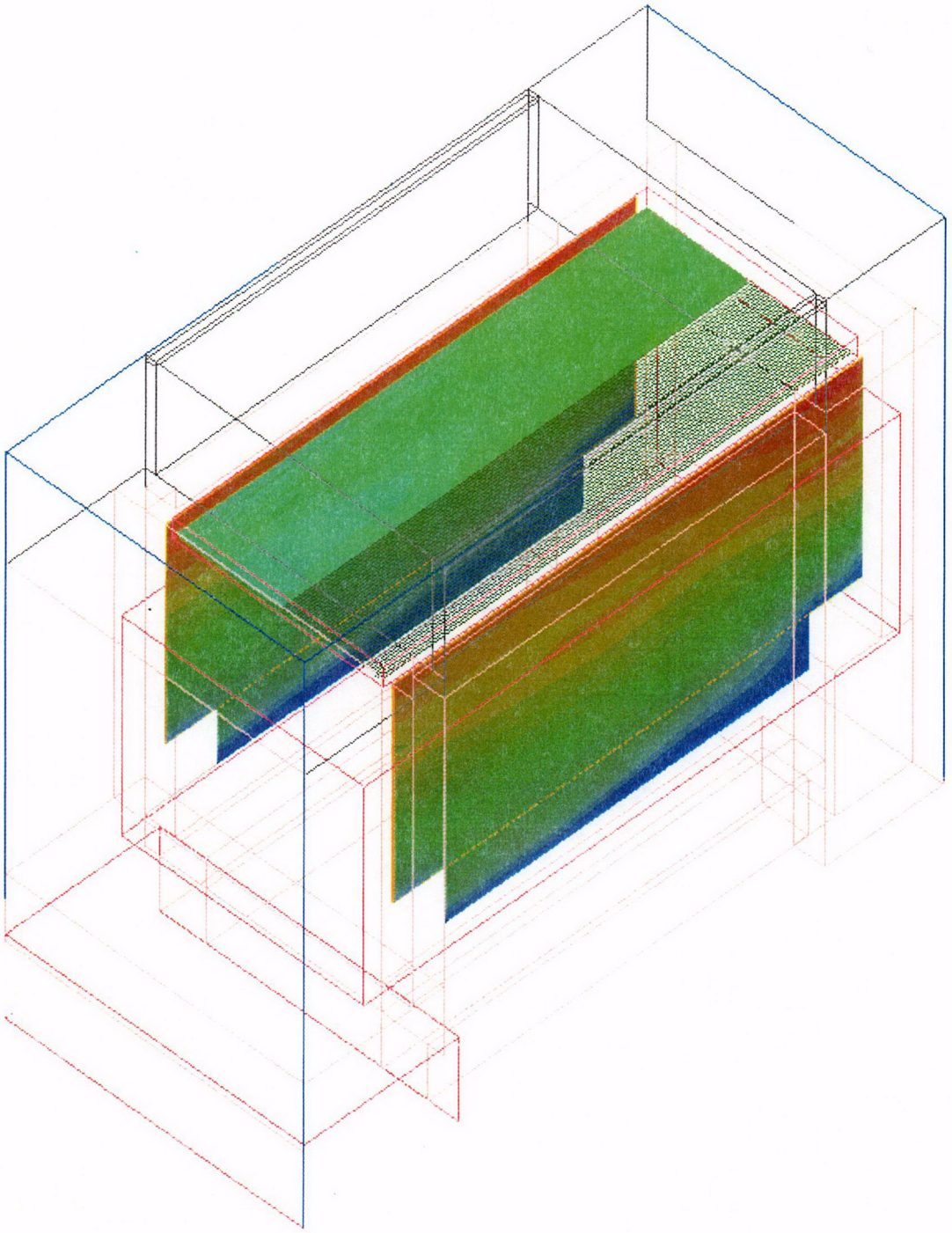

Figure 4-18 - Temperature Distribution On Heat shield Surfaces

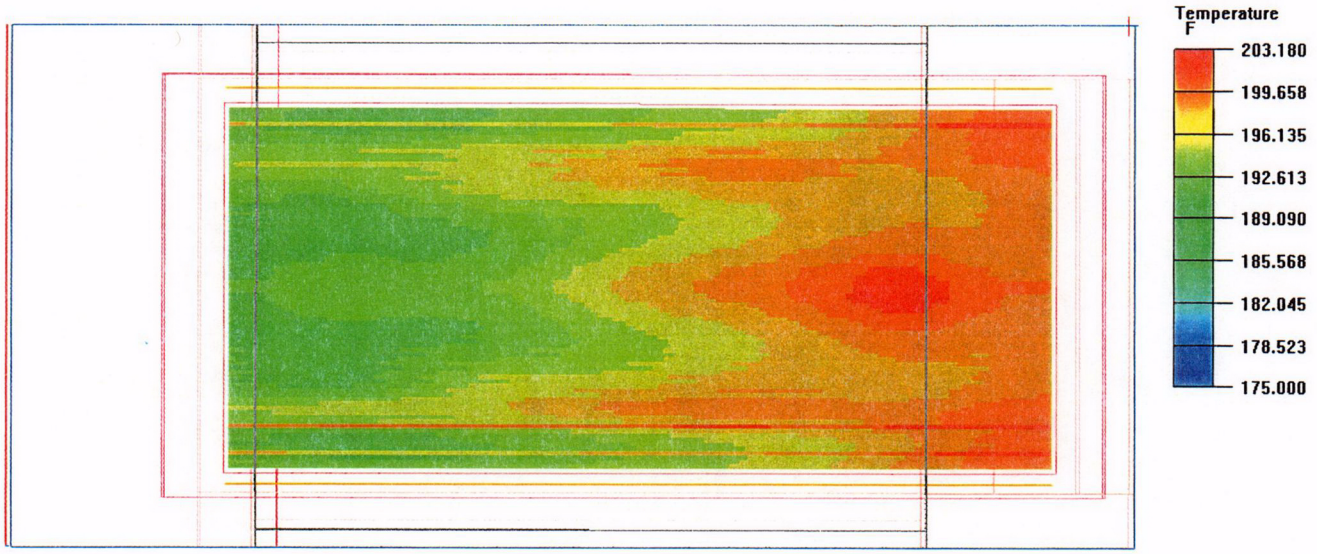

Figure 4-19 - Temperature Distribution On Louvered Heat shield

(Note: Front face of HSM-H module is to the left)

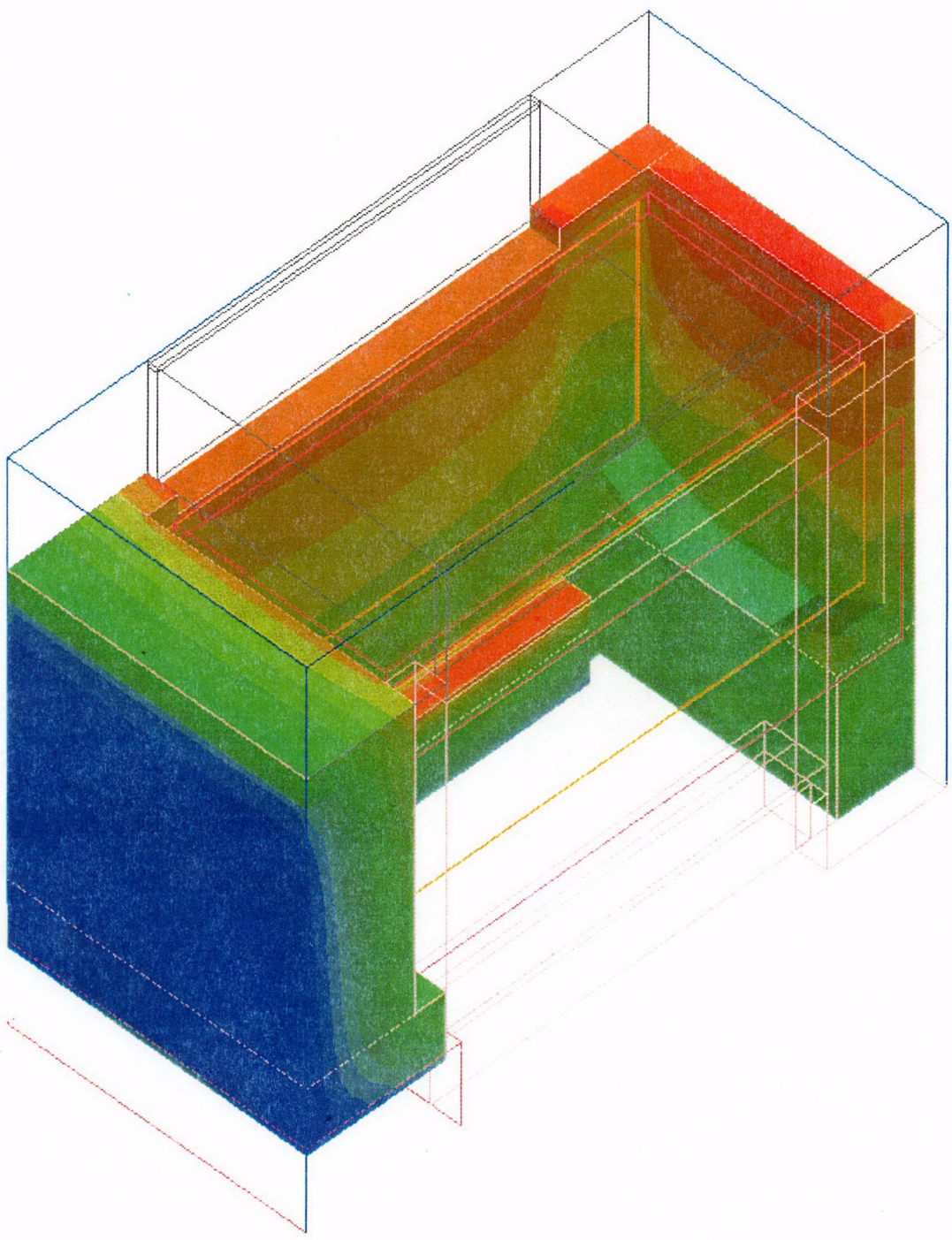

Figure 4-20 - Temperature Distribution On Concrete Surfaces Of Base Unit

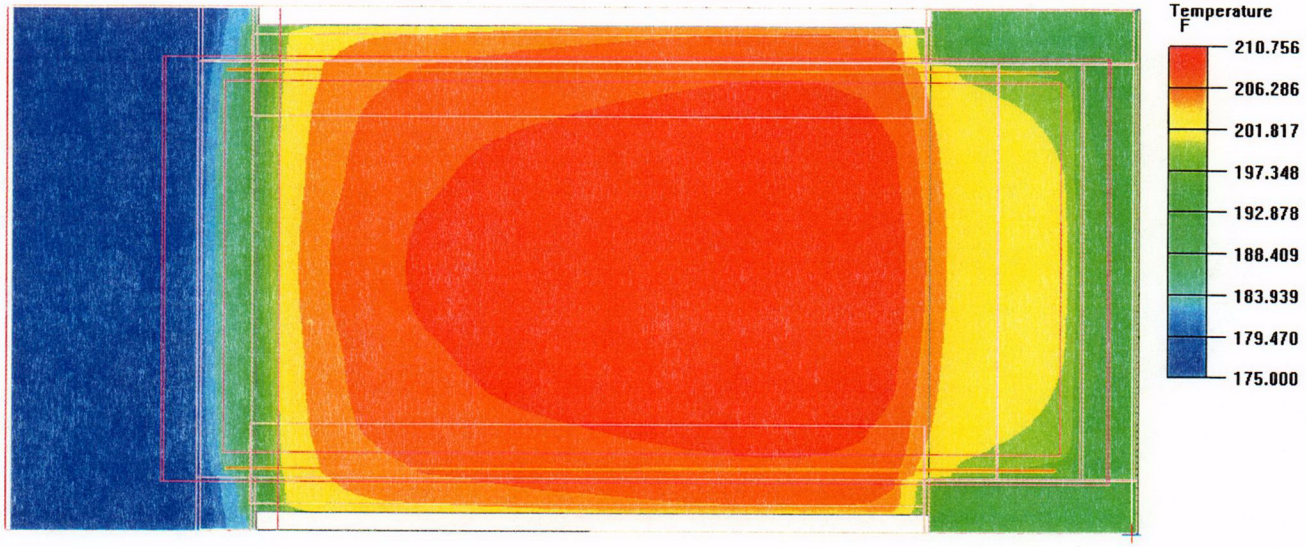

Figure 4-21 - Temperature Distribution On Underside Of Roof Structure

(Note: Front face of HSM-H module is to the left)

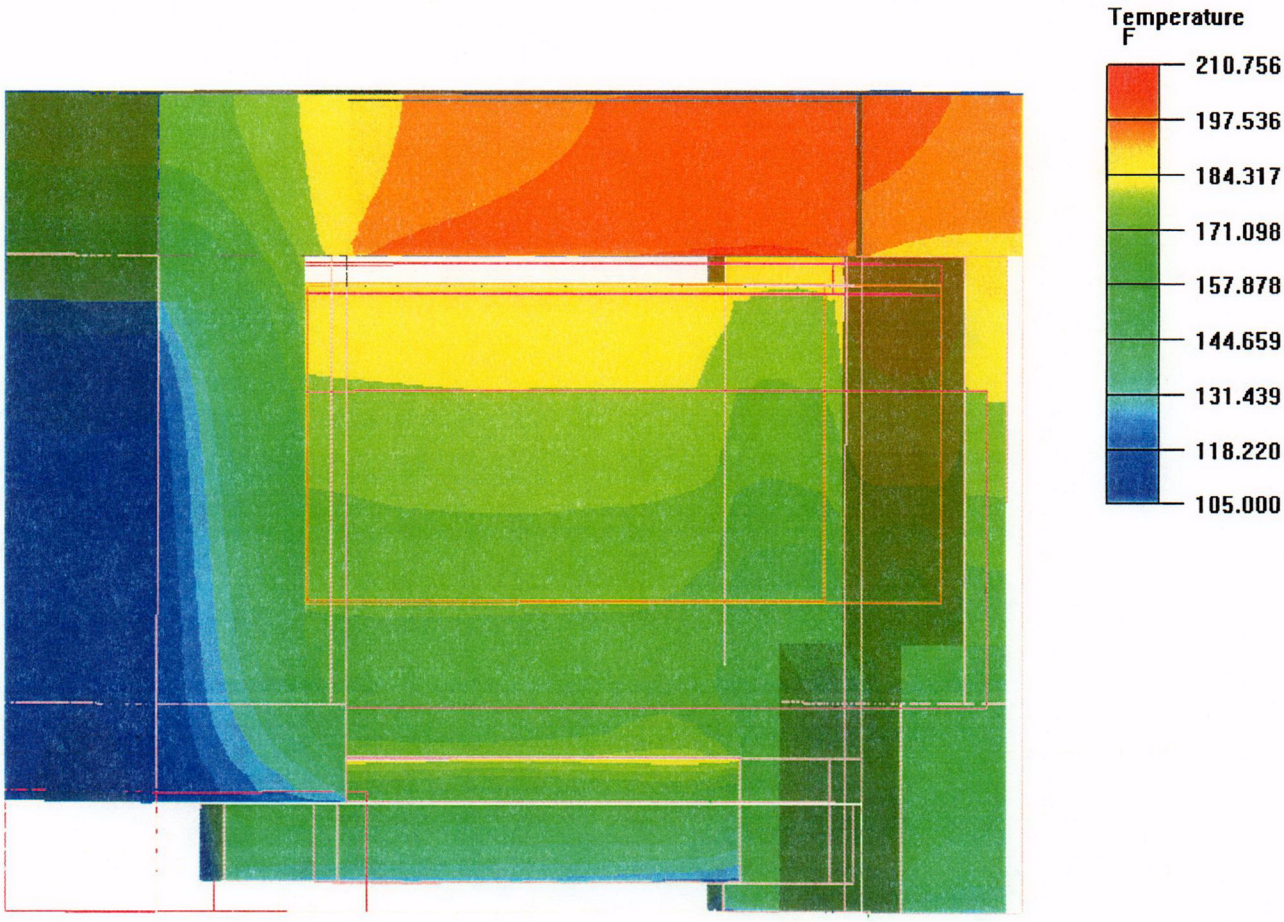

Figure 4-22 - Temperature Distribution On Concrete Surfaces

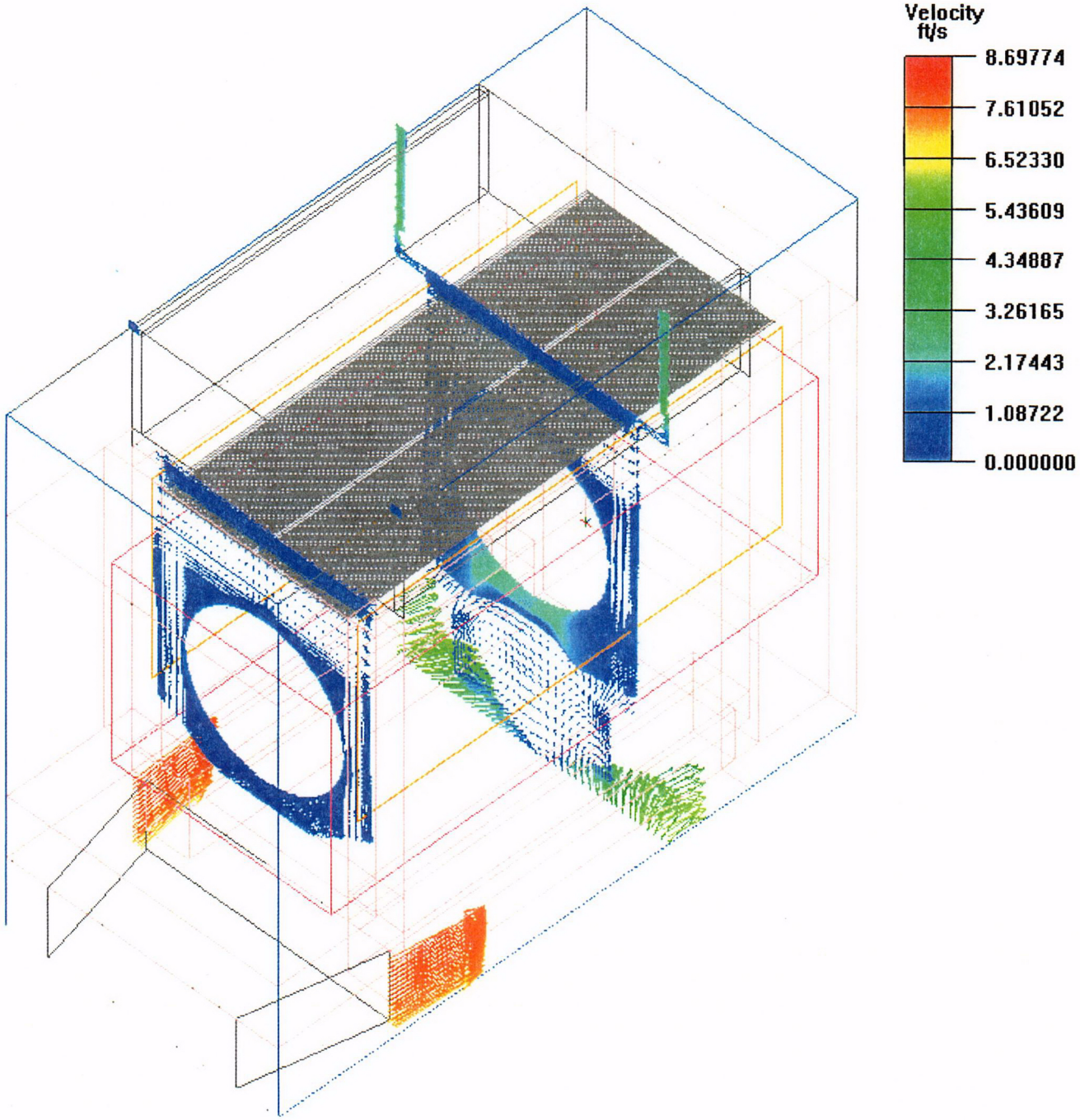

Figure 4-23 - Velocity Profile Along Two X-Y Planes Through HSM-H

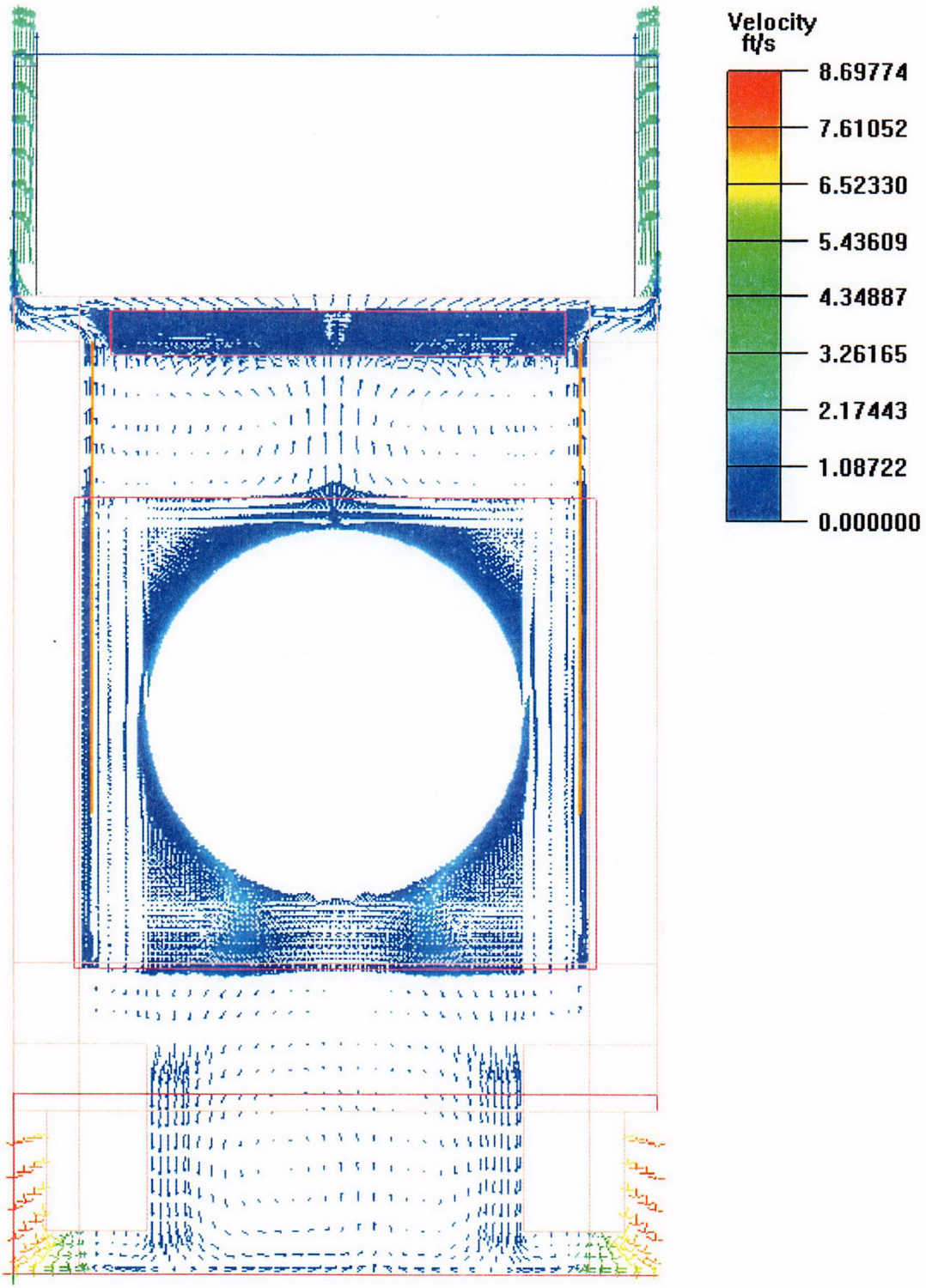

Figure 4-24 - Velocity Profile Along X-Y Plane At Center Of HSM-H

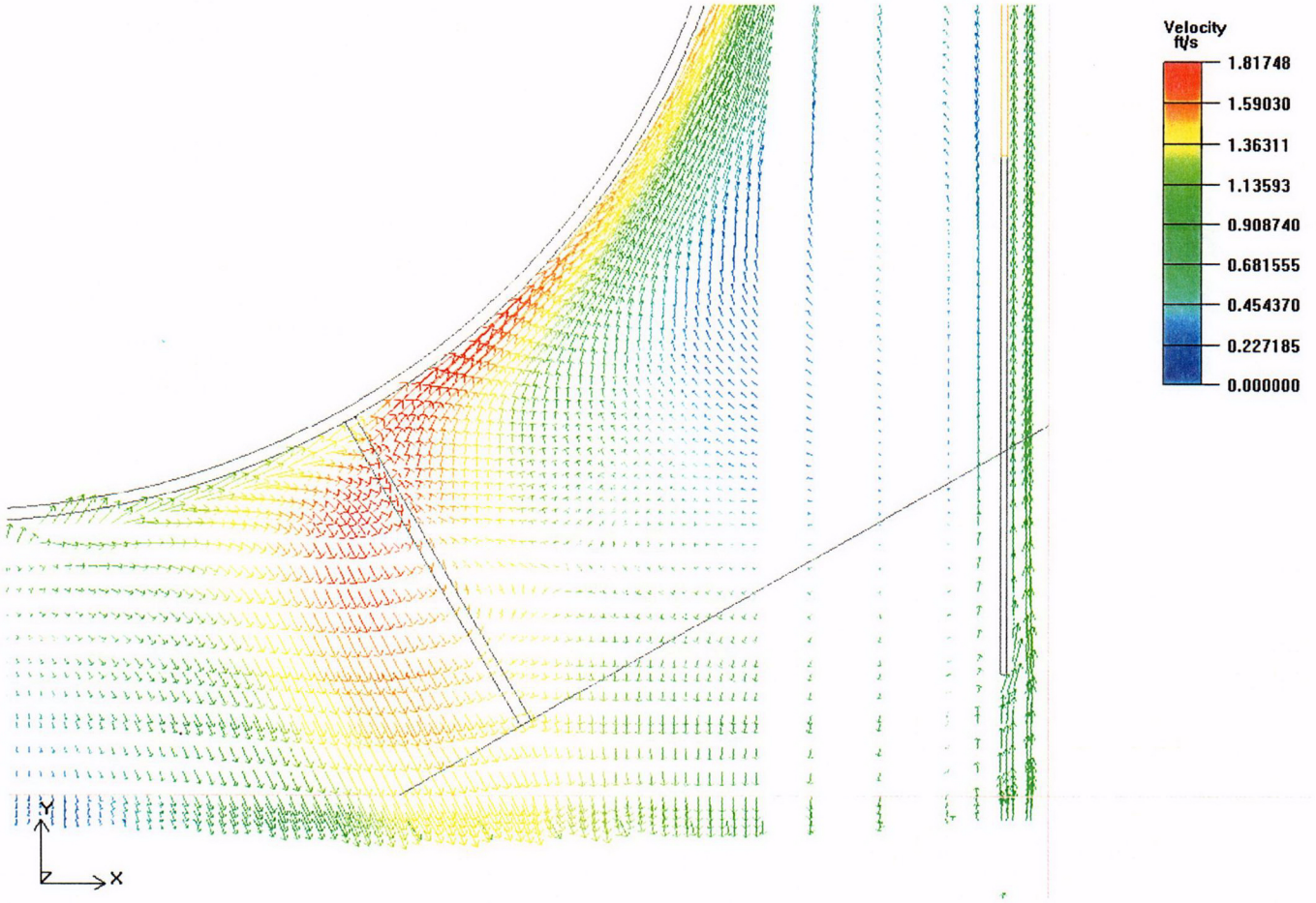

Figure 4-25 - Velocity Profile Along X-Y Plane And In The Region Of The DSC Support Rails At Center Of HSM-H

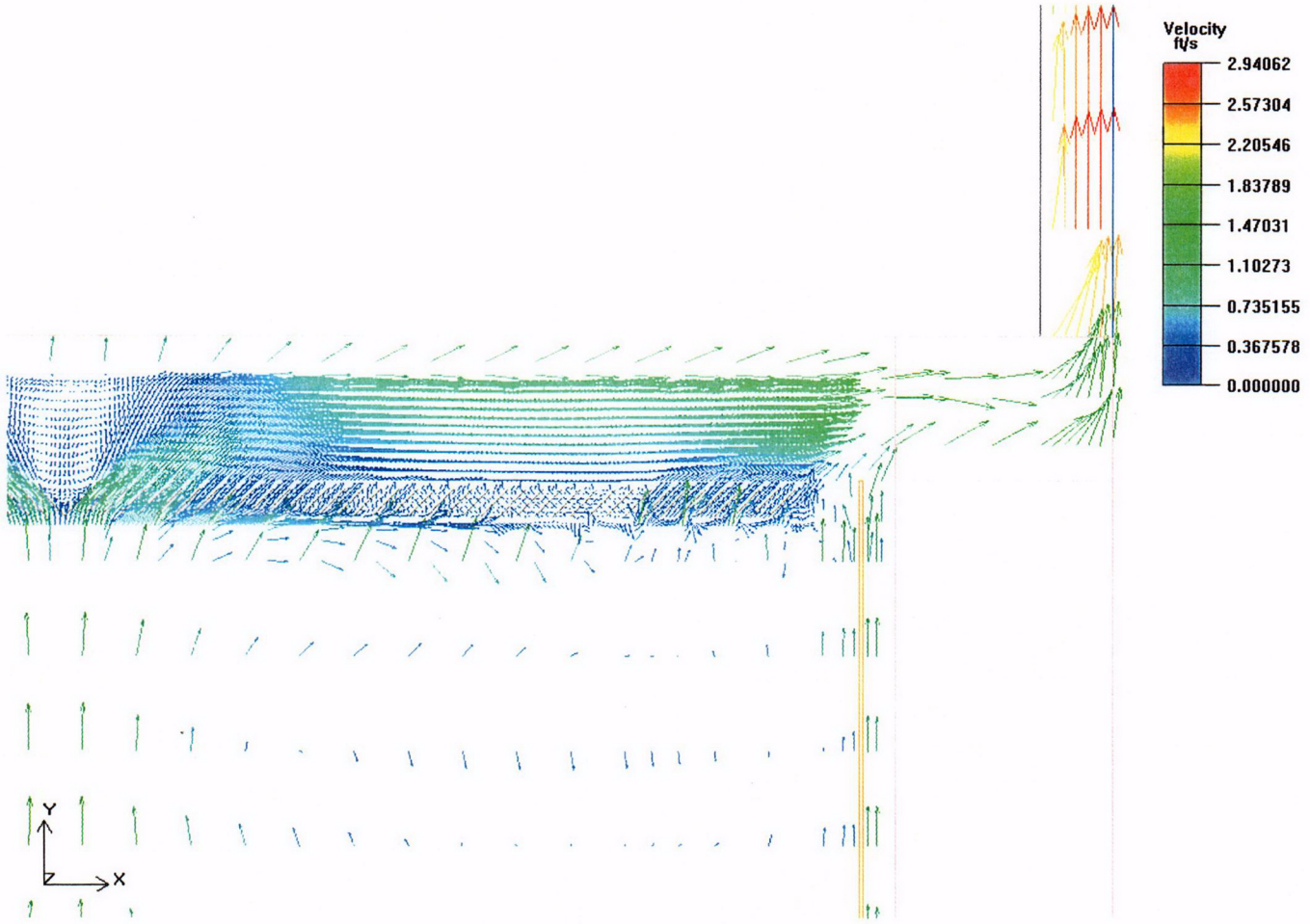

Figure 4-26 - Velocity Profile Along X-Y Plane And In The Region Of The Louver Heat Shield At Center Of HSM-H

5. SUMMARY AND CONCLUSION

A confirmatory evaluation of the thermal performance of the HSM-H module has been conducted using a computational fluid dynamics (CFD) methodology. The evaluation is meant to confirm the safety basis calculation provided in the [6.1] and [6.2] calculations. Table 5-1 summarizes the peak temperatures predicted by the different calculation methodologies used in each analysis. As seen from the table, generally good agreement is seen between the methodologies, with the CFD based methodology predicting lower peak surface temperatures on the DSC by approximately 20°F and essentially the same peak concrete within the base unit. The CFD based methodology does predict a higher peak roof concrete temperature than the [6.2] calculation by approximately 25°F, a hotter louvered (i.e., top) heat shield temperature by approximately 15°F, and a hotter side heat shield temperature by approximately 40°F.

The lower predicted DSC temperatures are assumed to be due to differences in the vertical profile of the air temperature within the HSM-H and differences in the computed convection coefficients. The [6.1] and [6.2] calculations assume a linear increase in the air temperature, whereas the computed temperature profile from the CFD analysis places greater increase in the air temperature near the top shield and module roof due to the cooling of these structures by the airflow as it passes. This conclusion is supported by the differences in the temperature profiles for the concrete walls and heat shield with vertical height, as predicted by the different methodologies.

The higher side heat shield temperature is directly related to ignoring of the approximately 10-fold increase in convective surface area which the fins provide on the side shields by the CFD analysis and to differences in the predicted vertical airflow temperature profiles. The higher peak temperature in the louvered heat shield is attributed to the differences in the airflow distribution across the heat shield and to differences in the vertical temperature profile. In keeping with its assumption of uniform flow and temperature profiles, the [6.2] analysis predicts a nearly flat temperature profile across the shield (i.e., 185.8 to 187.6°F). The average temperature of the shield as computed by the CFD analysis is 197°F.

The difference in the peak temperature of the roof concrete is due to differences in the computed view factors between the DSC and the underside of the roof through the louvered heat shield and partially due to differences in the flow distribution within the HSM. The [6.2] assumption of a fully mixed air temperature within each fluid zones does not factor in the 'plume' of hot air rising from the centerline of the DSC.

In conclusion, while some temperature differences exist between the CFD and the [6.1] and [6.2] calculations, the differences are understandable and related to the different methodologies used in the calculations. Further, each calculation methodology predicts results that are within the allowable material limits. As such, the results of the CFD calculation confirms the overall temperature levels and safety basis presented in the [6.1] and [6.2] calculations.

Table 5-1- Comparison Of Peak Component Temperatures Between [6.2] Analysis And This Confirmatory Calculation

Component	Results From [6.2] Analysis For 117°F Ambient With Fins	Confirmatory Calculation
DSC Shell	448°F	428°F
Base Unit Concrete	202°F	199°F
Roof Concrete	186°F	211°F
Top shield	188°F	203°F
Side Shield	181°F	220°F

6. REFERENCES

6.1 Transnuclear Calculation No. NUH24PTH.0420, *"NUHOMS®-24PTH Air Flow Calculation"*, Rev. 0.

6.2 Transnuclear Calculation No. NUH24PTH.0421, *"NUHOMS®-24PTH Thermal Analysis of the HSM"*, Rev. 0.

6.3 Drawing: Standardized NUHOMS® ISFSI HSM-H, Main Assembly, NUH-03.7001, Rev. 0.

6.4 ASME Boiler & Pressure Vessel Code, Section II, Part D, Properties, 1998 Edition including 2000 addenda.

6.5 I.E. Idelchik, *Handbook of Hydraulic Resistance*, 3rd Edition, 1994.

6.6 *FLUENT™*, Version 5.6, Fluent, Inc., Lebanon, NH, 2003.

6.7 *ICEPAK™*, Version 4.08, Fluent, Inc., Lebanon, NH, 2003.

6.8 Calculation NUH32PT.0414, *Validation of FLUENT™/ ICEPAK™ For Convective Flow In Enclosures*, Transnuclear April 2003, Rev. 0.

APPENDIX A: FLUENT™ / ICEPAK™ RUN LOG

The table below lists the associated with the FLUENT™ and ICEPAK™ associated computer files that defined the problem solved for this calculation. Due to the size of these files they can not be included in this appendix. Instead, the files are contained on an optical disk that accompanies this calculation.

FLUENT™ / ICEPAK™ Run Log

Case #	Operating Condition	File Name	Date
1	Off-Normal Hot Storage Condition, 117°F Peak Ambient, 40.8 kW Decay Heat Load	HSM_24PTH01.model HSM_24PTH01.problem HSM_24PTH01.job	8/29/2003 " "

APPENDIX B: COMPARISON RESULTS FROM [6.2] ANALYSIS

Temperature Distribution Results For 40.8kW, 117°F Ambient From [6.2]

DSC

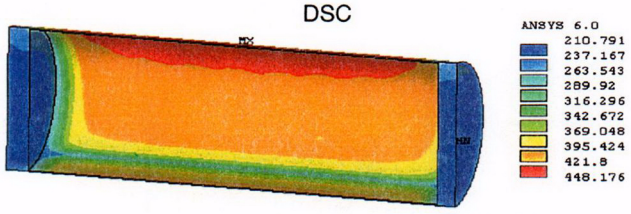

Top Heat Shield

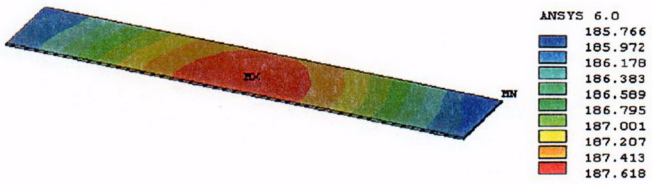

Support Rail

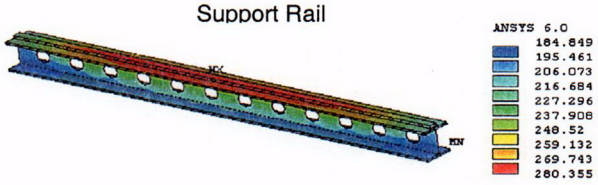

Side Heat Shield

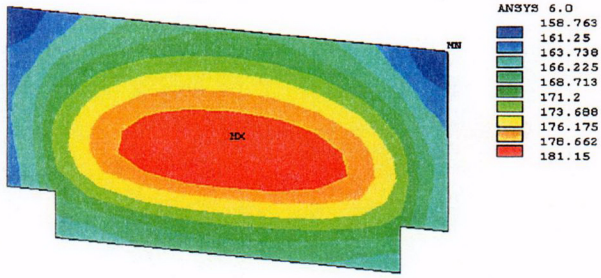

HSM